Plant cell wall patterning and expansion mediated by protein-peptide-polysaccharide interaction

Plant cell wall patterning and expansion mediated by protein-peptide-polysaccharide interaction

Steven Moussu[1†‡], Hyun Kyung Lee[1†], Kalina T. Haas[2], Caroline Broyart[1], Ursina Rathgeb,[3] Damien De Bellis[4,3], Thomas Levasseur[5], Sébastjen Schoenaers[2,6], Gorka S. Fernandez[7], Ueli Grossniklaus[7], Estelle Bonnin[5], Eric Hosy[8], Kris Vissenberg[6,9], Niko Geldner[3], Bernard Cathala[5], Herman Höfte[2]*, Julia Santiago[1]*

[1]The Plant Signaling Mechanisms Laboratory, Department of Plant Molecular Biology, University of Lausanne, 1015, Lausanne, Switzerland.

[2]Université Paris-Saclay, INRAE, AgroParisTech, Institut Jean-Pierre Bourgin (IJPB), 78000, Versailles, France.

[3]Department of Plant Molecular Biology, University of Lausanne, 1015 Lausanne, Switzerland.

[4]Electron Microscopy Facility, University of Lausanne, Lausanne, Switzerland.

[5] INRAE, UR1268 BIA, F-44300 Nantes, France.

[6]Integrated Molecular Plant Physiology Research (IMPRES), Department of Biology, University of Antwerp, Groenenborgerlaan 171, 2020 Antwerp, Belgium.

[7]Department of Plant and Microbial Biology & Zurich-Basel Plant Science Center, University of Zurich, 8008 Zurich, Switzerland.

[8]IINS, CNRS UMR5297, University of Bordeaux, 33000 Bordeaux, France

[9]Plant Biochemistry & Biotechnology Lab, Department of Agriculture, Hellenic Mediterranean University, Stavromenos PC 71410, Heraklion, Crete, Greece

[†] These authors contributed equally to this work

*Corresponding authors. Emails: hermanus.hofte@inrae.fr, julia.santiago@unil.ch

Abstract:

Assembly of cell wall polysaccharides into specific patterns is required for plant growth. A complex of RAPID ALKALINIZATION FACTOR4 (RALF4) and its cell wall-anchored LEUCINE-RICH REPEAT-EXTENSIN8 (LRX8) interacting protein is crucial for cell-wall integrity during pollen tube growth, but their molecular connection with the cell wall is unknown. Here, we show that LRX8-RALF4 complexes adopt a heterotetrametric configuration in vivo, displaying a dendritic distribution. The LRX8-RALF4 complex specifically interacts with demethylesterified pectins in a charge-dependent manner through RALF4's polycationic surface. The LRX8-RALF4-pectin interaction exerts a condensing effect, patterning the cell-wall polymers

into a reticulated network essential for cell wall integrity and expansion. Our work uncovers a dual structural and signaling mechanism for RALF4 in pollen tube growth and in the assembly of complex extracellular polymers.

One-Sentence Summary:

Pectin patterning through interaction with a protein-peptide complex is vital for pollen tube wall integrity and expansion.

A central question in plant biology is how cell wall polymers assemble into specific mesoscale patterns, conferring to the walls their physico-chemical properties that allow growth and development. Plant cell walls consist of cellulose microfibrils and matrix polymers, which include the polyanionic pectins. Among the pectins, homogalacturonan is the most abundant polymer in expanding cell walls (*1*). During cell expansion, regulation of homogalacturonan charge through demethylesterification plays a key role in controlling cell wall mechanics (*2–5*). Cell expansion needs to be tightly controlled by rapid feedback signaling loops that coordinate cell wall deposition and remodeling, to avoid loss of cell wall integrity. Here we show that RALF4 peptides are required for cell wall patterning through their interaction with demethylesterified homogalacturonan. RALFs were previously identified as signaling peptides that coordinate the functional integrity of cell walls in a plethora of processes underlying plant development and innate immunity *(6–14)*. These peptides instruct, in a mutually exclusive way and with different affinities, two structurally distinct protein families: the cell-wall anchored LRX proteins (*9*, *10*, *15*), and a membrane-integral signaling complex composed of LORELEI-like GLYCOLPHOSPHATIDYLINOSITOL (GPI)-ANCHORED PROTEINS (LLG) and *Catharanthus roseus* RLK1-like receptor kinases (*Cr*RLK1L) (*7*, *12*, *14*, *16*). In this study, we used the rapidly tip-growing pollen tube of *Arabidopsis thaliana* as a model system to investigate the molecular links between RALFs, LRX proteins and the cell wall matrix during cell expansion.

LRX-bound RALF4 interacts with charged homogalacturonan

Our previous structural analysis of the LRX8-RALF4 signaling complex in the pollen tube, revealed that RALF4 peptides, when bound to LRX8, expose an alkaline surface patch rich in Lys and Arg residues (*10*) (Fig. 1A). We hypothesized that this surface patch could serve as a platform to interact with negatively charged cell wall polysaccharides, such as pectins. The pollen tube

grows inside the pistil towards the ovule and must navigate through various tissues counterbalancing different physical forces (*17*, *18*). Along this journey, the cell wall at the pollen tube apex constantly needs to adjust its mechanical properties, to allow rapid growth whilst avoiding its rupture (*2*, *3*, *19*). Pectin charge plays a key role in this process (*3–5*).

We initially compared the melting profile of recombinantly expressed LRX8 and LRX8-RALF4 complexes (*10*) in the presence and absence of fully demethylesterified homogalacturonan fragments (6-15- mer oligogalacturonans, hereafter referred as OGs) in thermal shift assays (*20*) (Fig. 1B and C, and fig. S1). Thermal shift assays revealed, in line with our isothermal titration calorimetry (ITC) experiments, an increase in melting temperature (T_m) of LRX8 upon binding to RALF4 (Fig. 1B and C) (*10*). The T_m further increased in the presence of OGs, while no such changes were observed for LRX8 alone (Fig. 1B and C, and fig. S1). In addition, the LRX8-RALF4 complex did not bind shorter homogalacturonan fragments (fig. S1), a structurally divergent acidic polysaccharide (polymannuronic acid), a negatively charged polymer (DNA), or an unrelated carbohydrate (sucrose) (Fig. 1D, and fig. S1). We next quantified these interactions, by titrating OGs into an LRX8-RALF4 solution (*10*), using isothermal titration calorimetry (*21*). LRX8-RALF4 bound OGs at ~ 2 μM affinity and a binding stoichiometry (N) of 2, suggesting that one OG molecule binds to each of the two RALF4 molecules in the heterotetrametric (2+2) LRX8-RALF4 complex (*10*) (Fig. 1E, and fig. S2). Consistently, a monomeric version of the complex, monomericLRX8-RALF4 (*10*)(*13*), bound 1 OG molecule (N=1) with comparable affinity (~ 2.9 μM), and its T_m increased in the presence of OGs (Fig. 1E, and fig. S2). The non-pollen-tube expressed LRX2 protein in complex with RALF4, bound OGs with a similar dissociation constant (1.6 μM) and stoichiometry (Fig. 1E, and fig. S2). No binding was detected when titrating OGs into a solution containing either LRX8 alone or free RALF4; or when titrating DNA into the LRX8-RALF4 complex (Fig. 1E, and fig. S2). These experiments demonstrate that the LRX-RALF4 complex can bind homogalacturonan oligomers with high affinity and specificity.

During pollen tube growth, demethylesterification at the apex changes the overall electrostatic charge of homogalacturonan, which plays a role in controlling cell-wall expansion (*3*, *5*, *22*). The degree of methylation (DM) of homogalacturonan was critical for the interaction with LRX8-RALF4 as shown by its increased thermostability in the presence of non- or low-methylesterified (DM5= 5% methylesterified) OGs (increase in T_m of 3.9° and 2.5° degrees, respectively), but not of highly methylesterified ones (DM71) (Fig. 1F, and fig. S2). Similar results were obtained when using longer pectin chains: the shift in T_m for DM20 pectin occurred at lower concentrations

compared to DM43 pectins (Fig. 1G, and fig. S2). These results show that LRX8-RALF4 specifically interacts with demethylesterified pectins.

To understand the interaction between LRX8-RALF4 and demethylesterified pectins in molecular terms, we mapped and probed the basic surface of the LRX8-bound RALF4 peptide (*10*) (Fig. 1A). We mutated residues in RALF4's basic patch either to alanine or glutamic acid, and recombinantly expressed two mutant variants of the LRX8-RALF4 complex: one targeting the protruding loop of the folded signaling peptide ($RALF4_{R89E.R90E.R91E}$), and the other neutralizing the basic surface altogether ($RALF4_{K70A.R78A.K87A.K88A.R89A.R90A.R91A.R96A}$; hereafter referred as $RALF4_{neutral\ surface}$) (Fig. 1A, and fig. S3). Both RALF4 mutants still bound LRX8 and LLG3 with wild type-like affinity (fig. S3) (*10*). However, thermal shift assays failed to detect an OG-induced increase in T_m for both LRX8-bound RALF4 mutants (Fig. 1B-D, 1I and fig. S4). Consistent with these findings, LRX8-$RALF4_{neutral\ surface}$ and LRX8-$RALF4_{R89E.R90E.R91E}$ showed no, or a ~ 4-fold reduced OG-binding relative to the wild-type complex in isothermal titration calorimetry assays, respectively (Fig. 1E, 1J and fig. S4). Together, these results confirm the electrostatic nature of the interaction between LRX8-RALF4 and pectin.

LRX8, RALF4 and pectin form a reticulated pattern in vivo

Next, we investigated whether LRX8, RALF4, and pectin also interact in vivo. To this end we carried out immunolabelling and high-resolution microscopy on pollen tubes expressing functionally-tagged RALF4-HA and LRX8-myc under their native promoters (fig. S5) (*10*). In line with our structural and biochemical data (*10*), both proteins co-localized in pollen tube cell-walls, suggesting that the complex is also present in vivo. However, the complex was present all along the pollen tube cell wall (Fig. 2A, and fig. S6) and not just at the tip, where the peptide and LRX8 are secreted. This indicates that LRX8 and RALF4, become an integral part of the pollen tube cell wall; an unexpected finding for a signaling peptide. This was confirmed by dSTORM super-resolution microscopy (*23*, *24*), showing a comparable distribution for the RALF4-HA peptide and LRX8-myc in punctate domains forming a reticulated network (Fig. 2B and 2D). Moreover, cluster-size analysis of LRX8-myc and RALF4-HA was consistent with the presence of either one or two copies of the tags in each puncta, indicating the presence of heterotetrametric complexes in vivo (Fig. 2C and 2E) (*10*). Concerning the distribution of demethylesterified homogalacturonan, Airyscan and dSTORM microscopy showed that the LM19 immunolabel for demethylesterified pectin (*25*) was not distributed randomly, as expected for an amorphous pectin gel, but formed an

interconnected pattern of fibers (Fig. 2F, 2G, and fig. S7 and S8) (*26*, *27*). This observed architecture is reminiscent of previously described ring-like pectin bands in pollen tubes (*28*, *29*). The pattern presented a bimodal angle distribution, displaying as LRX8-RALF4, a web-like network (Fig. 2F, 2G and 2H, and fig. S7 and S8). The interaction of LRX8-RALF4 with demethylesterified homogalacturonan in vivo was corroborated by the colocalization of RALF4-HA with LM19 antibodies in a periodic banding pattern at the pollen tube surface (Fig. 2I). This was confirmed at higher resolution by dSTORM microscopy, where a two-point correlation function analysis showed that domains containing LM19-labelled pectin and RALF4-HA were not distributed independently of each other but were associated in space, exhibiting a reticulated pattern (Fig. 2J and fig. S9).

Cell wall patterning and integrity through LRX8-RALF4-pectin compaction

The reticulated pattern could indicate the association of LRX8-RALF4 with pre-existing fibrous structures or a more active role of the complex in the patterning of the cell wall polysaccharides. To investigate the latter possibility, we first studied in vitro how exposure to LRX8-RALF4 affects the rheology of a pectin layer, using Quartz-Crystal Microbalance with Dissipation monitoring (QCM-D) (*21*, *30*). Briefly, to prepare the pectin layer, a pectin solution (DM43) was poured over an oscillating quartz crystal coated with a polycationic polymer, while monitoring the frequency (ΔF, negative for a mass increase) and dissipation rate of the oscillation upon interruption of the current (ΔD, positive for increase in viscoelasticity of the layer). The drop in ΔF and increase in ΔD indicated the formation of an elastic pectin layer (Fig. 3A and fig. S10). Addition of free RALF4 induced an increase in ΔF rather than a decrease expected for the binding of the peptide, and a strong decrease in ΔD. This is consistent with an electrostatic interaction between the cationic RALF4 and anionic pectin, causing the hydrated pectin layer to dewater and stiffen. The increase in ΔF indicates that the mass loss due to dewatering, exceeds the mass gain due to the binding of the small 5.6 kDa peptide. The RALF4-pectin interaction was reversible as shown by the slow reversal of ΔF and ΔD during a subsequent washing step (Fig. 3B and fig. S10). Addition of LRX8-RALF4 to the pectin layer resulted in an amplified decrease in ΔF and ΔD (Fig. 3B). Here the mass increase of the much larger complex (110 kDa) exceeded the mass of the expulsed water, explaining the decrease in ΔF. The complex, in contrast to the free RALF4 peptide, had a lasting condensing effect on the pectin layer since ΔF and ΔD did not reverse during the washing step (Fig. 3B). Consistent with our previous binding assays, LRX8 alone did not induce any changes

either in frequency (binding) or pectin rigidification, confirming that RALF4 targets the complex to pectins. It is of note, that the monomerized LRX8-RALF4 complex also induced pectin stiffening (negative ΔD) but showed a greatly reduced pectin binding capacity (ΔF) relative to the dimeric protein (Fig. 3C), suggesting functional differences depending on the oligomeric state of the complex. The charge dependence of the pectin interaction was confirmed by the strongly reduced pectin binding and condensing capacity of LRX8-RALF4$_{\text{neutral surface}}$ (Fig. 3D).

These results demonstrate that LRX8-RALF4 has the capacity to recognize and condense demethylesterified pectins in a charge-dependent way. To investigate whether this capacity may direct the patterning of the pollen-tube cell wall and impact cell expansion, we generated complementation lines of the *amiralf4/19* line (*9*) by expressing amiRNA-resistant versions of RALF4$_{\text{WT}}$, RALF4$_{\text{R89E.R90E.R91E}}$ and RALF4$_{\text{neutral surface}}$ under the control of the native RALF4 promoter (fig. S11). The two RALF4 variants co-localized with LRX8 in the cell wall (fig. S5 and S12). While RALF4$_{\text{WT}}$ fully restored pollen tube growth and fertility of the *amiralf4/19* line, the RALF4$_{\text{R89E.R90E.R91E}}$ and RALF4$_{\text{neutral surface}}$ conferred, moderate or severe reduction in fertility and pollen tube growth in vivo, respectively (Fig. 3E-H), but nevertheless maintained their capacity to direct their growth towards the ovules (*31*). The growth defect of *amiralf4/19* pollen tubes reflected a higher (not lower) growth velocity and premature bursting rate. Both parameters were only partially complemented in the lines expressing RALF4$_{\text{R89E.R90E.R91E}}$ or RALF4$_{\text{neutral surface}}$ (fig. S13). In addition, in these lines, a large proportion of the surviving pollen tubes did not show continuous oscillatory growth (*32*), but a stop-and-go growth pattern often followed by bursting (Fig. 3I-J). Similar growth phenotypes were observed in the pollen LRX mutants (*33*) and in a mutant (*ppme1*) with impaired pectin demethylesterification (*5*, *34*) (fig. S14). These data suggest that the interaction of LRX-RALF4 with demethylesterified pectin is critical for pollen tube cell wall integrity and growth.

To investigate the impact of impaired pectin interaction on cell wall patterning, we studied the cell walls of surviving pollen tubes in *amiralf4/19* complemented lines with RALF4$_{\text{neutral surface}}$. Immunolabelling experiments showed a wild-type spatial localization of pectin epitopes in *amiralf4/19 pRALF4::RALF4*$_{\textit{neutral surface}}$ lines, with high DM (LM20 antibody) and no DM (LM19 antibody) pectins at the pollen tube tip and shank, respectively (fig. S15) (*3*, *25*). Interestingly, dSTORM microscopy on *amiralf4/19 pRALF4:RALF4*$_{\textit{neutral surface}}$ cell walls, labeled for low DM pectins (LM19), showed a denser array of punctae (Fig. 3K-L) relative to the wild-type that lacked

filamentous features (Fig. 2G-H, and fig. S8). Transmission electron microscopy (TEM) on transverse sections through the shank of pollen tubes of both wild-type and *amiralf4/19* RALF4$_{WT}$ complementation lines revealed a compact cell wall with a thin inner secondary cell wall layer labeled with anti-callose antibodies. A thicker and unstructured pectic cell wall filled with patches of callose was observed in *amiralf4/19* pollen tubes (Fig. 4A, and fig. S16). Notably, expression of RALF4$_{neutral\ surface}$ did not restore a wild-type cell wall architecture while RALF4$_{R89E.R90E.R91E}$ partially complemented the aberrant discontinuous structural pattern albeit maintaining the thick callose layer and a fibrous, more loosely packed outer cell wall (Fig. 4A and fig. S16). Altogether, these results show that RALF4 is not only a signaling peptide, but also a structural cell wall component, promoting the patterning of cell wall polysaccharides into a strong polymer assembly, as part of the LRX8-RALF4-pectin complex.

Discussion

In this study, we show that cell wall polysaccharides are shaped into a reticulated network through a peptide-activated LRX8 complex that binds and condenses pectins, thus becoming an integral part of the cell wall and conferring integrity to the expandable cell wall during pollen tube growth (Fig. 4B and fig. S17). The pectin homogalacturonan, despite the considerable differences between the mechanical landscapes of plant cell walls and the animal extracellular matrix, can be considered the equivalent of animal glycosaminoglycans (GAGs). GAGs are also unbranched and charged polysaccharides that undergo compaction and rigidification via the interaction with GAG-binding cross-linking proteins (*35*, *36*). LRX8-RALF4 is a polysaccharide-binding protein complex that promotes mesoscale cell wall patterning. The particularity of this complex, as opposed to known GAG-binding proteins, lies in its modularity, with a polycationic peptide activating the LRX8 cell-wall protein to bind polyanionic pectic polysaccharides. The LRX8-RALF4-pectin interaction appears to be essential for cell wall patterning and pollen tube growth in plants. This is shown by the failure of the RALF4$_{R89E.R90E.R91E}$ and RALF4$_{neutral\ surface}$ variants to restore normal cell wall organization, growth and fertility to *amiralf4/19* pollen tubes, where the severity of the complemented phenotype scales with the severity of the homogalacturonan-binding defect.

The RALF4 peptide is molded through its interaction with LRX8 thus exposing, at the surface of the heterotetramer, 2 patches of cationic residues with an affinity for polyanionic homogalacturonan. The charge-dependent compaction of the pectin matrix may combine

polyelectrolyte complex formation (also observed for the unstructured free peptide) and homogalacturonan crosslinking by the LRX8-RALF4 heterotetramer. The latter is suggested by the reduced binding capacity of the pectin layer for monomerized LRX8-RALF4 (shown by QCM-D), relative to the native complex; despite a comparable affinity of isolated OGs as shown by calorimetry and thermal shift assays. This property might be critical for LRX8-RALF4 bioactivity, given the unability of the LRX8 monomer to complement the fertility phenotype of the *lrx* quadruple mutant (*10*). Pollen tube growth involves a balancing act between cell wall assembly, consolidation and turgor-driven wall expansion (*2*, *3*). We propose that the web-like LRX-RALF-pectin network constitutes a load-bearing component of the pollen tube cell wall, perhaps compensating for its low cellulose content (*3*, *37*). Disruption of this network causes the pollen tube to burst, in particular during the transition from the style into the transmitting tract (*18*). In this context it is notable that LRX proteins comprise, besides a RALF-binding Leucine Rich Repeat (LRR) domain, an extensin domain (*10*, *33*, *38*). Extensins are hydroxyproline-rich, periodically amphiphilic proteins, often with YXY motifs that can form extensin peroxidase-catalyzed, di-isodityrosine intermolecular cross-links with other extensins (*39–42*). At least one extensin (AtEXT3) has been shown to form a dendritic scaffold in vitro. Due to the polybasic nature of AtEXT3, it was hypothesized that this scaffold may structure the cell wall by creating pectin-extensin coacervates, which may be consolidated by oxidative crosslinking between extensins (*43*). The extensin domain of LRX8 contains cross-linking acceptor tyrosine residues but it is much less charged than AtEXT3 (17 His residues vs 91 His/Lys in AtEXT3). We propose that LRX8 co-opts the positive charges of the polybasic RALF4 peptide to mediate specific pectin interactions. This modularity has two obvious advantages. Firstly, it creates the possibility to target the LRX-extensin network to different cell wall polymers or polymer motifs by exchanging the RALF peptide. A large variety of RALF peptides have the capacity to bind to the conserved binding pocket of LRX proteins, exposing distinct surface patches (*10*). This could contribute to the patterning of celltype-specific cell walls or cell-wall domains with different architectures such as the reticulated homogalacturonan network shown in onion cell walls or the pectin nanofilaments in epidermal cells (*27*, *44*). Secondly, it would allow rapid regulation of cell wall assembly by monitoring free RALF peptides, which may feed-back to cellular processes that control actin dynamics as well as secretion and modification of cell wall polymers via the low-affinity LLG/BUPS/ANX receptor complexes (*12*, *16*, *45–52*). Future studies could investigate under which conditions free RALF peptides are released or transferred to instruct the *Cr*RLK1Ls and

LRX complexes, and how this informs the cell on the status of the cell wall assembly process during cell expansion and morphogenesis. In one possible scenario, pectin could connect LLG/*Cr*RLK1L to LRX-RALF complexes, thus forming a mechanosensing cell wall network (*45*). Supporting this scenario, a direct interaction between pectin and *Cr*RLK1Ls has been reported (*53*). This interaction is most likely weak, at least for the *Cr*RLK1Ls ANX1 and BUPS1, since it escaped detection by calorimetry or thermal shift assays (*20*, *21*) when tested with different OGs or polygalacturonic acid (fig. S18) (*54*). Nevertheless, such a weak interaction might be suitable to support a role in mechanosensing, for instance by detecting the deformation of the LRX-RALF-pectin network. This study uncovers the unique dual signaling and structural role of RALF4 in shaping cell wall assembly during cell expansion and morphogenesis and may provide inspiration to uncover additional roles for protein-polysaccharide interactions in defining cell wall architecture and properties.

References

1. M. A. Atmodjo, Z. Hao, D. Mohnen, Evolving Views of Pectin Biosynthesis. *Annual Review of Plant Biology*. **64**, 747–779 (2013).

2. P. Fayant, O. Girlanda, Y. Chebli, C.-É. Aubin, I. Villemure, A. Geitmann, Finite Element Model of Polar Growth in Pollen Tubes. *The Plant Cell*. **22**, 2579–2593 (2010).

3. Y. Chebli, M. Kaneda, R. Zerzour, A. Geitmann, The Cell Wall of the Arabidopsis Pollen Tube—Spatial Distribution, Recycling, and Network Formation of Polysaccharides. *Plant Physiology*. **160**, 1940–1955 (2012).

4. E. Parre, A. Geitmann, Pectin and the role of the physical properties of the cell wall in pollen tube growth of Solanum chacoense. *Planta*. **220**, 582–592 (2005).

5. N. Röckel, S. Wolf, B. Kost, T. Rausch, S. Greiner, Elaborate spatial patterning of cell-wall PME and PMEI at the pollen tube tip involves PMEI endocytosis, and reflects the distribution of esterified and de-esterified pectins. *Plant J*. **53**, 133–143 (2008).

6. G. Pearce, D. S. Moura, J. Stratmann, C. A. Ryan, RALF, a 5-kDa ubiquitous polypeptide in plants, arrests root growth and development. *Proceedings of the National Academy of Sciences*. **98**, 12843–12847 (2001).

7. M. Haruta, G. Sabat, K. Stecker, B. B. Minkoff, M. R. Sussman, A Peptide Hormone and Its Receptor Protein Kinase Regulate Plant Cell Expansion. *Science*. **343**, 408–411 (2014).

8. E. Murphy, L. D. Vu, L. Van den Broeck, Z. Lin, P. Ramakrishna, B. van de Cotte, A. Gaudinier, T. Goh, D. Slane, T. Beeckman, D. Inzé, S. M. Brady, H. Fukaki, I. De Smet, RALFL34 regulates formative cell divisions in Arabidopsis pericycle during lateral root initiation. *Journal of Experimental Botany*. **67**, 4863–4875 (2016).

9. M. A. Mecchia, G. Santos-Fernandez, N. N. Duss, S. C. Somoza, A. Boisson-Dernier, V. Gagliardini, A. Martínez-Bernardini, T. N. Fabrice, C. Ringli, J. P. Muschietti, U. Grossniklaus, RALF4/19 peptides interact with LRX proteins to control pollen tube growth in Arabidopsis. *Science*. **358**, 1600–1603 (2017).

10. S. Moussu, C. Broyart, G. Santos-Fernandez, S. Augustin, S. Wehrle, U. Grossniklaus, J. Santiago, Structural basis for recognition of RALF peptides by LRX proteins during pollen tube growth. *Proceedings of the National Academy of Sciences*. **117**, 7494–7503 (2020).

11. M. Gonneau, T. Desprez, M. Martin, V. G. Doblas, L. Bacete, F. Miart, R. Sormani, K. Hématy, J. Renou, B. Landrein, E. Murphy, B. Van De Cotte, S. Vernhettes, I. De Smet, H. Höfte, Receptor Kinase THESEUS1 Is a Rapid Alkalinization Factor 34 Receptor in Arabidopsis. *Current Biology*. **28**, 2452-2458.e4 (2018).

12. Z. Ge, T. Bergonci, Y. Zhao, Y. Zou, S. Du, M.-C. Liu, X. Luo, H. Ruan, L. E. García-Valencia, S. Zhong, S. Hou, Q. Huang, L. Lai, D. S. Moura, H. Gu, J. Dong, H.-M. Wu, T. Dresselhaus, J. Xiao, A. Y. Cheung, L.-J. Qu, Arabidopsis pollen tube integrity and sperm release are regulated by RALF-mediated signaling. *Science*. **358**, 1596–1600 (2017).

13. S. Schoenaers, D. Balcerowicz, G. Breen, K. Hill, M. Zdanio, G. Mouille, T. J. Holman, J. Oh, M. H. Wilson, N. Nikonorova, L. D. Vu, I. De Smet, R. Swarup, W. H. De Vos, I. Pintelon, D. Adriaensen, C. Grierson, M. J. Bennett, K. Vissenberg, The Auxin-Regulated CrRLK1L Kinase ERULUS Controls Cell Wall Composition during Root Hair Tip Growth. *Curr Biol*. **28**, 722-732.e6 (2018).

14. M. Stegmann, J. Monaghan, E. Smakowska-Luzan, H. Rovenich, A. Lehner, N. Holton, Y. Belkhadir, C. Zipfel, The receptor kinase FER is a RALF-regulated scaffold controlling plant immune signaling. *Science*. **355**, 287–289 (2017).

15. A. Herger, S. Gupta, G. Kadler, C. M. Franck, A. Boisson-Dernier, C. Ringli, Overlapping functions and protein-protein interactions of LRR-extensins in Arabidopsis. *PLOS Genetics*. **16**, e1008847 (2020).

16. Z. Ge, Y. Zhao, M.-C. Liu, L.-Z. Zhou, L. Wang, S. Zhong, S. Hou, J. Jiang, T. Liu, Q. Huang, J. Xiao, H. Gu, H.-M. Wu, J. Dong, T. Dresselhaus, A. Y. Cheung, L.-J. Qu, LLG2/3 Are Co-receptors in BUPS/ANX-RALF Signaling to Regulate Arabidopsis Pollen Tube Integrity. *Current Biology*. **29**, 3256-3265.e5 (2019).

17. B. C. W. Crawford, G. Ditta, M. F. Yanofsky, The NTT Gene Is Required for Transmitting-Tract Development in Carpels of Arabidopsis thaliana. *Current Biology*. **17**, 1101–1108 (2007).

18. I. Fobis-Loisy, Y. Jaillais, Feeling the pressure: A mechanical tale of the pollen tube journey through the pistil. *Developmental Cell*. **56**, 873–875 (2021).

19. A. Geitmann, How to shape a cylinder: pollen tube as a model system for the generation of complex cellular geometry. *Sex Plant Reprod*. **23**, 63–71 (2010).

20. C. J. Layton, H. W. Hellinga, Quantitation of protein–protein interactions by thermal stability shift analysis. *Protein Sci*. **20**, 1439–1450 (2011).

21. P. J. Sandoval, J. Santiago, In Vitro Analytical Approaches to Study Plant Ligand-Receptor Interactions1 [OPEN]. *Plant Physiology*. **182**, 1697–1712 (2020).

22. M. Bosch, A. Y. Cheung, P. K. Hepler, Pectin methylesterase, a regulator of pollen tube growth. *Plant Physiol*. **138**, 1334–1346 (2005).

23. E. Betzig, G. H. Patterson, R. Sougrat, O. W. Lindwasser, S. Olenych, J. S. Bonifacino, M. W. Davidson, J. Lippincott-Schwartz, H. F. Hess, Imaging intracellular fluorescent proteins at nanometer resolution. *Science*. **313**, 1642–1645 (2006).

24. M. J. Rust, M. Bates, X. Zhuang, Sub-diffraction-limit imaging by stochastic optical reconstruction microscopy (STORM). *Nat Methods*. **3**, 793–795 (2006).

25. Y. Verhertbruggen, S. E. Marcus, A. Haeger, J. J. Ordaz-Ortiz, J. P. Knox, An extended set of monoclonal antibodies to pectic homogalacturonan. *Carbohydr Res*. **344**, 1858–1862 (2009).

26. K. Palacio-Lopez, L. Sun, R. Reed, E. Kang, I. Sørensen, J. K. C. Rose, D. S. Domozych, Experimental Manipulation of Pectin Architecture in the Cell Wall of the Unicellular Charophyte, Penium Margaritaceum. *Front Plant Sci*. **11**, 1032 (2020).

27. K. T. Haas, R. Wightman, E. M. Meyerowitz, A. Peaucelle, Pectin homogalacturonan nanofilament expansion drives morphogenesis in plant epidermal cells. *Science*. **367**, 1003–1007 (2020).

28. F. Dardelle, A. Lehner, Y. Ramdani, M. Bardor, P. Lerouge, A. Driouich, J.-C. Mollet, Biochemical and immunocytological characterizations of Arabidopsis pollen tube cell wall. *Plant Physiol*. **153**, 1563–1576 (2010).

29. Y.-Q. Li, H.-Q. Zhang, E. S. Pierson, F.-Y. Huang, H. F. Linskens, P. K. Hepler, M. Cresti, Enforced growth-rate fluctuation causes pectin ring formation in the cell wall of Lilium longiflorum pollen tubes. *Planta*. **200**, 41–49 (1996).

30. M. C. Dixon, Quartz Crystal Microbalance with Dissipation Monitoring: Enabling Real-Time Characterization of Biological Materials and Their Interactions. *J Biomol Tech*. **19**, 151–158 (2008).

31. S. Okuda, H. Tsutsui, K. Shiina, S. Sprunck, H. Takeuchi, R. Yui, R. D. Kasahara, Y. Hamamura, A. Mizukami, D. Susaki, N. Kawano, T. Sakakibara, S. Namiki, K. Itoh, K. Otsuka, M. Matsuzaki, H. Nozaki, T. Kuroiwa, A. Nakano, M. M. Kanaoka, T. Dresselhaus, N. Sasaki, T. Higashiyama, Defensin-like polypeptide LUREs are pollen tube attractants secreted from synergid cells. *Nature*. **458**, 357–361 (2009).

32. J. A. Feijó, J. Sainhas, T. Holdaway-Clarke, M. S. Cordeiro, J. G. Kunkel, P. K. Hepler, Cellular oscillations and the regulation of growth: the pollen tube paradigm. *Bioessays*. **23**, 86–94 (2001).

33. T. N. Fabrice, H. Vogler, C. Draeger, G. Munglani, S. Gupta, A. G. Herger, P. Knox, U. Grossniklaus, C. Ringli, LRX Proteins Play a Crucial Role in Pollen Grain and Pollen Tube Cell Wall Development. *Plant Physiology*. **176**, 1981–1992 (2018).

34. G.-W. Tian, M.-H. Chen, A. Zaltsman, V. Citovsky, Pollen-specific pectin methylesterase involved in pollen tube growth. *Dev Biol*. **294**, 83–91 (2006).

35. R. P. Richter, N. S. Baranova, A. J. Day, J. C. Kwok, Glycosaminoglycans in extracellular matrix organisation: are concepts from soft matter physics key to understanding the formation of perineuronal nets? *Current Opinion in Structural Biology*. **50**, 65–74 (2018).

36. J. J. Walkowiak, M. Ballauff, R. Zimmermann, U. Freudenberg, C. Werner, Thermodynamic Analysis of the Interaction of Heparin with Lysozyme. *Biomacromolecules*. **21**, 4615–4625 (2020).

37. H. Schlupmann, A. Bacic, S. M. Read, Uridine Diphosphate Glucose Metabolism and Callose Synthesis in Cultured Pollen Tubes of Nicotiana alata Link et Otto. *Plant Physiology*. **105**, 659–670 (1994).

38. C. Ringli, The hydroxyproline-rich glycoprotein domain of the Arabidopsis LRX1 requires Tyr for function but not for insolubilization in the cell wall. *The Plant Journal*. **63**, 662–669 (2010).

39. J. D. BRADY, I. H. SADLER, S. C. FRY, Di-isodityrosine, a novel tetrametric derivative of tyrosine in plant cell wall proteins: a new potential cross-link. *Biochemical Journal*. **315**, 323–327 (1996).

40. M. A. Held, L. Tan, A. Kamyab, M. Hare, E. Shpak, M. J. Kieliszewski, Di-isodityrosine Is the Intermolecular Cross-link of Isodityrosine-rich Extensin Analogs Cross-linked in Vitro*. *Journal of Biological Chemistry*. **279**, 55474–55482 (2004).

41. S. Moussu, G. Ingram, The EXTENSIN enigma. *The Cell Surface*. **9**, 100094 (2023).

42. D. T. A. Lamport, M. J. Kieliszewski, Y. Chen, M. C. Cannon, Role of the Extensin Superfamily in Primary Cell Wall Architecture1. *Plant Physiol*. **156**, 11–19 (2011).

43. M. C. Cannon, K. Terneus, Q. Hall, L. Tan, Y. Wang, B. L. Wegenhart, L. Chen, D. T. A. Lamport, Y. Chen, M. J. Kieliszewski, Self-assembly of the plant cell wall requires an extensin scaffold. *Proceedings of the National Academy of Sciences*. **105**, 2226–2231 (2008).

44. W. J. Nicolas, F. Fäßler, P. Dutka, F. K. M. Schur, G. Jensen, E. Meyerowitz, Cryo-electron tomography of the onion cell wall shows bimodally oriented cellulose fibers and reticulated homogalacturonan networks. *Curr Biol*. **32**, 2375-2389.e6 (2022).

45. X. Zhou, J. Lu, Y. Zhang, J. Guo, W. Lin, J. M. Van Norman, Y. Qin, X. Zhu, Z. Yang, Membrane receptor-mediated mechano-transduction maintains cell integrity during pollen tube growth within the pistil. *Dev Cell*. **56**, 1030-1042.e6 (2021).

46. N. Luo, A. Yan, G. Liu, J. Guo, D. Rong, M. M. Kanaoka, Z. Xiao, G. Xu, T. Higashiyama, X. Cui, Z. Yang, Exocytosis-coordinated mechanisms for tip growth underlie pollen tube growth guidance. *Nat Commun*. **8**, 1687 (2017).

47. A. Boisson-Dernier, D. S. Lituiev, A. Nestorova, C. M. Franck, S. Thirugnanarajah, U. Grossniklaus, ANXUR Receptor-Like Kinases Coordinate Cell Wall Integrity with Growth at the Pollen Tube Tip Via NADPH Oxidases. *PLOS Biology*. **11**, e1001719 (2013).

48. L. Zhu, L.-C. Chu, Y. Liang, X.-Q. Zhang, L.-Q. Chen, D. Ye, The Arabidopsis CrRLK1L protein kinases BUPS1 and BUPS2 are required for normal growth of pollen tubes in the pistil. *The Plant Journal*. **95**, 474–486 (2018).

49. Y. J. Lee, A. Szumlanski, E. Nielsen, Z. Yang, Rho-GTPase–dependent filamentous actin dynamics coordinate vesicle targeting and exocytosis during tip growth. *Journal of Cell Biology*. **181**, 1155–1168 (2008).

50. S. T. McKenna, J. G. Kunkel, M. Bosch, C. M. Rounds, L. Vidali, L. J. Winship, P. K. Hepler, Exocytosis precedes and predicts the increase in growth in oscillating pollen tubes. *Plant Cell*. **21**, 3026–3040 (2009).

51. Y. Gu, Y. Fu, P. Dowd, S. Li, V. Vernoud, S. Gilroy, Z. Yang, A Rho family GTPase controls actin dynamics and tip growth via two counteracting downstream pathways in pollen tubes. *J Cell Biol*. **169**, 127–138 (2005).

52. Y. Gu, V. Vernoud, Y. Fu, Z. Yang, ROP GTPase regulation of pollen tube growth through the dynamics of tip-localized F-actin. *Journal of Experimental Botany*. **54**, 93–101 (2003).

53. W. Feng, D. Kita, A. Peaucelle, H. N. Cartwright, V. Doan, Q. Duan, M.-C. Liu, J. Maman, L. Steinhorst, I. Schmitz-Thom, R. Yvon, J. Kudla, H.-M. Wu, A. Y. Cheung, J. R. Dinneny, The FERONIA Receptor Kinase Maintains Cell-Wall Integrity during Salt Stress through Ca2+ Signaling. *Current Biology*. **28**, 666-675.e5 (2018).

54. S. Moussu, S. Augustin, A.-O. Roman, C. Broyart, J. Santiago, Crystal structures of two tandem malectin-like receptor kinases involved in plant reproduction. *Acta Cryst D*. **74**, 671–680 (2018).

55. M. Futatsumori-Sugai, K. Tsumoto, Signal peptide design for improving recombinant protein secretion in the baculovirus expression vector system. *Biochem Biophys Res Commun*. **391**, 931–935 (2010).

56. Y. Hashimoto, S. Zhang, S. Zhang, Y.-R. Chen, G. W. Blissard, Correction: BTI-Tnao38, a new cell line derived from Trichoplusia ni, is permissive for AcMNPV infection and produces high levels of recombinant proteins. *BMC Biotechnol*. **12**, 12 (2012).

57. E. Bonnin, E. Dolo, A. Le Goff, J.-F. Thibault, Characterisation of pectin subunits released by an optimised combination of enzymes. *Carbohydr Res*. **337**, 1687–1696 (2002).

58. K. Huynh, C. L. Partch, *Curr Protoc Protein Sci*, in press, doi:10.1002/0471140864.ps2809s79.

59. H. K. Lee, S. Macgregor, D. R. Goring, "A Toolkit for Teasing Apart the Early Stages of Pollen–Stigma Interactions in Arabidopsis thaliana" in *Pollen and Pollen Tube Biology: Methods and Protocols*, A. Geitmann, Ed. (Springer US, New York, NY, 2020; https://doi.org/10.1007/978-1-0716-0672-8_2), *Methods in Molecular Biology*, pp. 13–28.

60. D. R. Smyth, J. L. Bowman, E. M. Meyerowitz, Early flower development in Arabidopsis. *Plant Cell*. **2**, 755–767 (1990).

61. L. Nahidiazar, A. V. Agronskaia, J. Broertjes, B. van den Broek, K. Jalink, Optimizing Imaging Conditions for Demanding Multi-Color Super Resolution Localization Microscopy. *PLOS ONE*. **11**, e0158884 (2016).

62. A. Peaucelle, R. Wightman, K. T. Haas, Multicolor 3D-dSTORM Reveals Native-State Ultrastructure of Polysaccharides' Network during Plant Cell Wall Assembly. *iScience*. **23**, 101862 (2020).

63. K. T. Haas, A. Peaucelle, Protocol for multicolor three-dimensional dSTORM data analysis using MATLAB-based script package Grafeo. *STAR Protocols*. **2**, 100808 (2021). (https://github.com/inatamara/Grafeo-dSTORM-analysis-).

Acknowledgments: We would like to thank Alexis Peaucelle for constant and insightful discussions along the project development. dSTORM experiments were performed at the Curie Institute, Paris, and at Interdisciplinary Institute for Neurocience (IINS), Bordeaux, and we thank David Mazaud, Patricia le Baccon, and Daniel Choquet for their support.

Funding:

University of Lausanne (J.S.)

European Research Council (ERC) grant agreements WallWatchers no. 716358 (J.S.)

Swiss National Science Foundation grant no. 310030_204526 (J.S.)

French Bio-Imaging (FBI) no. 2411 (K.T.H.)

Funded by the European Union ERC STORMtheWALL grant agreement no.101041597 (K.T.H.)

Agence Nationale de Recherche (ANR) grant "Homeowall" (H.H.)

Saclay Plant Sciences-SPS (ANR-17-EUR-0007) (H.H., K.T.H.)

Research Foundation Flanders (FWO; grants 1225120N and G013023N), University of Antwerp (UA; BOF-KP) and BOF-DOCPRO4 (K.V.)

LASERLAB-EUROPE (grant no. 654148) (S.S.)

Swiss National Science Foundation grant no. CR32I3_156724 (U.G.)

Author contributions: S.M and H.K.L. conceptualization, methodology, investigation, visualization and data analysis. J.S. and S.M. performed the structural analysis and design the RALF4 mutants. S.M. generated all the transgenic lines reported in the study. S.M and H.K.L performed the pollen tube growth assays, TSA and ITC assays, immunostaining experiments and prepared samples for dSTORM, AiryScan and TEM imaging, and prepared figures: Fig 1, Fig. 2A and 2I, Fig. 3, 3E-J, and 4A-D and the associated supplementary information. K.T.H. acquired and analyzed dSTORM data and prepared the associated figures. C.B purified proteins and performed ITC assays and prepared the corresponding figures. U.R acquired and analyzed Airyscan data and prepared the associated figures (Fig. 2F and S7). D. De Bellis performed the TEM sectioning, immuno-detection of callose and acquired the TEM data images. T. L. and E.B. prepared pectins and OGs with different DMs. G.S-F. generated the first generation of in vivo RALF4 mutants. U.G. provided materials and supervised initial work on the first generation of in vivo RALF4 mutants. S.S. participated in the optimization of pollen tube growth behavior. K.V. supervised the the optimization of pollen tube growth behavior. E. H. provided dSTORM support. N.G. supervised the Airyscan data acquisition and analysis. B.C provided with the QCMD expertise and supported data analysis. H.H. performed the QCMD experiments and data analysis, and prepared associated figures. J.S. and H.H.: conceptualization, supervision, funding acquisition and project administration. J.S and H.H wrote the original draft. All the authors reviewed and edited the manuscript.

Competing interests: Authors declare that they have no competing interests.

Data and materials availability: All data are available in the main text or the supplementary materials. Materials from this paper are available through the corresponding authors upon request.

Supplementary Materials

Materials and Methods

Figs. S1 to S18

References (*55*–*63*)

Fig. .1 **LRX-bound RALF4 specifically interacts with demethylesterified homogalacturonan in a charge-dependent manner.**

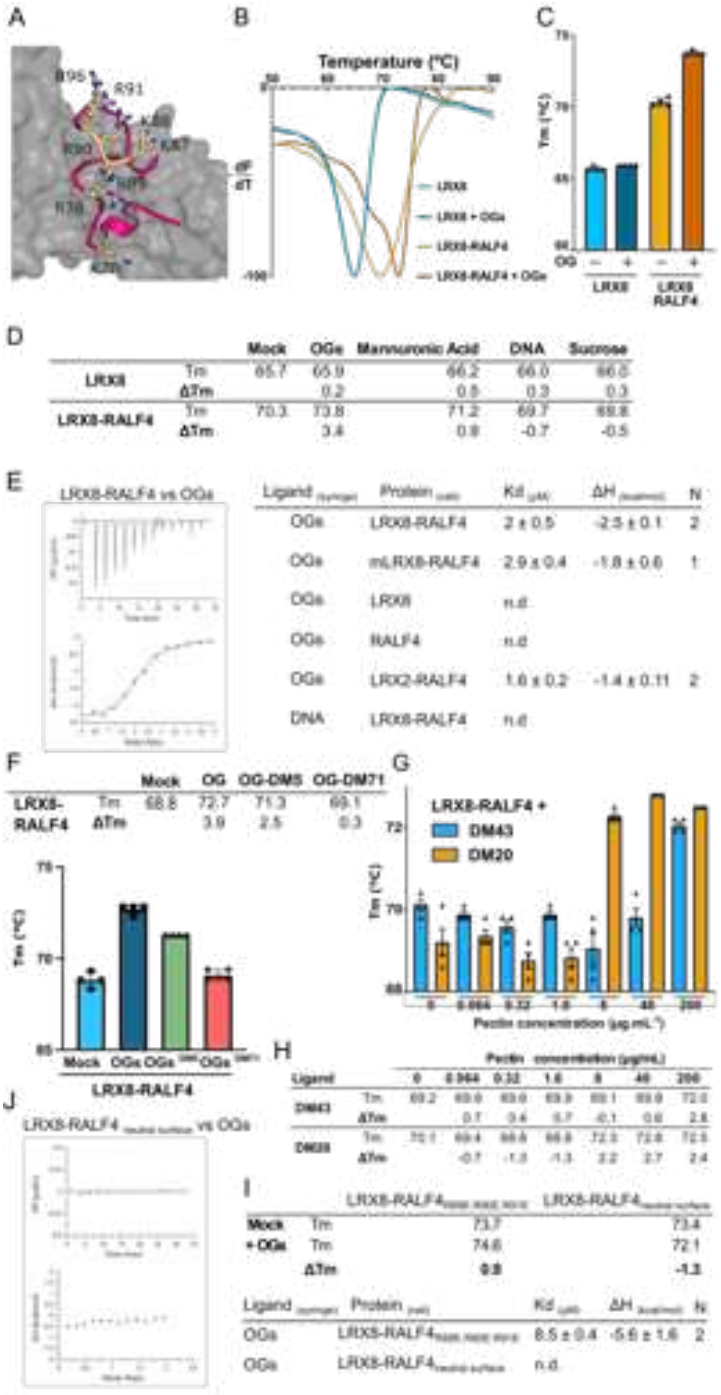

5

Fig 1. **LRX-bound RALF4 specifically interacts with demethylesterified homogalacturonan in a charge-dependent manner.** (A) Structural representation of the polycationic interface of RALF4 when bound to LRX8 (PDB: 6QWN). LRX8 is depicted in surface representation (grey) and RALF4 as pink ribbon diagram. Positively charged amino acids in the exposed RALF4 interface are depicted as yellow sticks. (B) LRX8-bound RALF4 binds demethylesterified homogalacturonan. Representative thermal denaturation profiles of LRX8 and LRX8-RALF4 in the absence and presence of OGs. (C) Graphical representation of melting temperatures (T_m) of different thermal shift assays shown in (B). Data are means ± SD of 4 independent experiments. (D) Summary table of T_m and ΔT_m of LRX8 and LRX8-RALF4 in the presence of OGs and control molecules; n=4. (E) ITC thermogram of LRX8-RALF4 vs OGs (left), and ITC summary table (right) of LRX8 alone, RALF4 and LRXs-RALF4 vs OGs and DNA oligomers. K_d, (dissociation constant) indicates the binding affinity between the two molecules considered (in micromolar). The N indicates the reaction stoichiometry (n = 1 for a 1:1 interaction). The values indicated in the table are the mean ± SD of at least two independent experiments. n.d = no detectable binding. (F) Summary table (top) and representation of melting temperatures (bottom) of LRX8-RALF4 vs OGs and OGs with different degrees of methylesterification (ex. DM71=71% methylesterification). Data are means ± SD, n=4. (G) T_ms bar representation of LRX8-RALF4 in the presence of increasing concentrations of long chains of homogalacturonan with DM43 and DM20. Data are means ± SD, n=4. (H) Summary table of the T_ms shown in panel (G). (I and J) Mutation of RALF4 polycationic surface disrupts the interaction with homogalacturonan. (I) Summary table of T_ms of RALF4 $_{R89E.R90E.R91E}$ and RALF4 $_{neutral\ surface}$ variants in the presence of OGs. (J) ITC of RALF4 $_{neutral\ surface}$ vs OGs (left). (Right) ITC summary table of RALF4 $_{R89E.R90E.R91E}$ and RALF4 $_{neutral\ surface}$ mutants vs OGs. The values indicated in the table are the mean ± SD of at least two independent experiments. n.d. = no detectable binding.

Fig 2. **LRX8, RALF4 and pectin associate in vivo and form a reticulated pattern.**

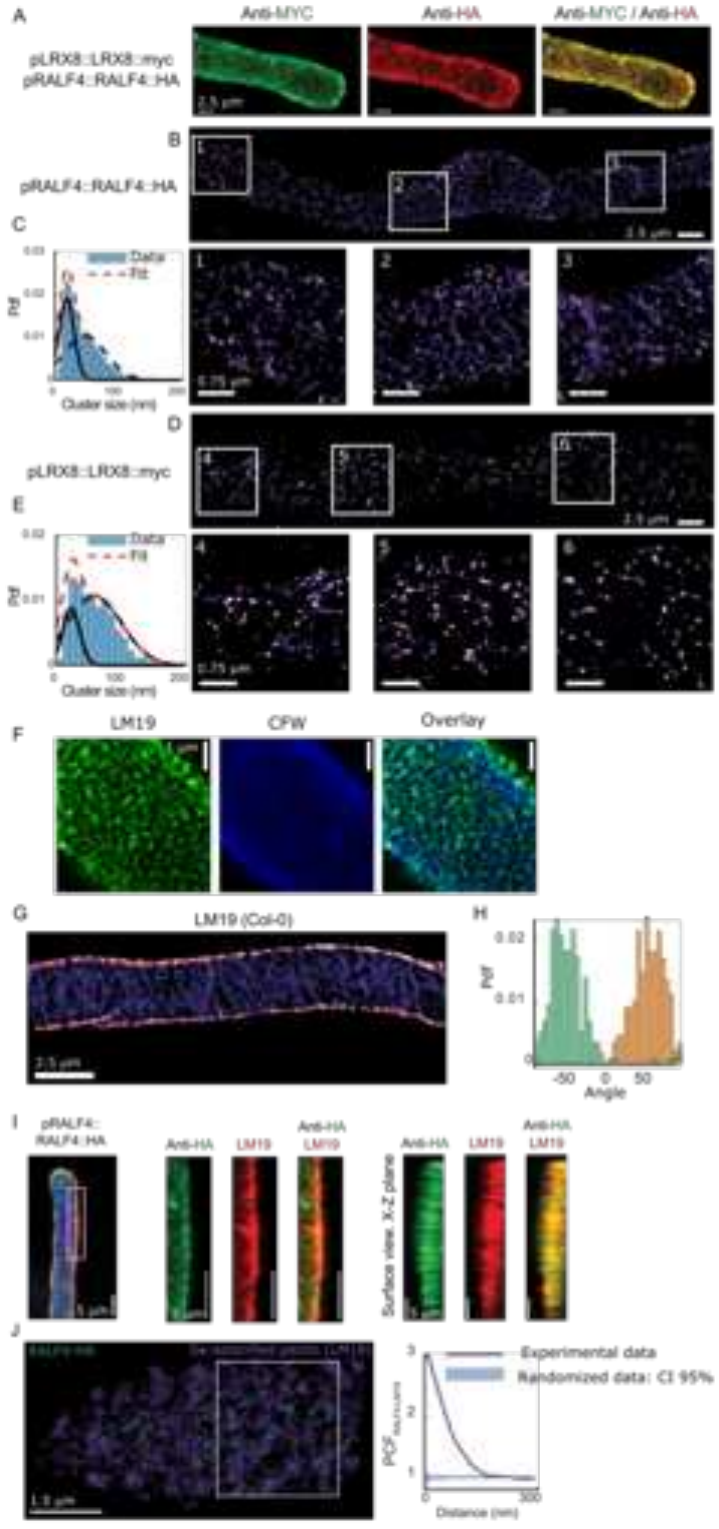

5

Fig 2. **LRX8, RALF4 and pectin associate in vivo and form a reticulated pattern.** (A) Representative immunolabeled pollen tube images of a transgenic line expressing LRX8-myc and RALF4-HA under their native promoter in the Col-0 accession. (B) Representative pollen tube dSTORM image of immunolabelled *pRALF4::RALF4::HA* in Col-0. (bottom) Zoom in on the corresponding squared regions marked in the pollen tube shank shown above. (C) Histogram of RALF4-HA probability density function (Pdf) vs cluster size (blue). Fit of the Gaussian mixture model shows two cluster populations with a mean size of 18 nm (monomer 35%) and 47 nm (dimers 65%). 1137 clusters were analyzed from 7 pollen tubes from 4 plants. (D) Representative pollen tube dSTORM image of immunolabelled *pLRX8::LRX8::myc* in Col-0 background. (bottom) Zoom in on the corresponding squared regions marked in the pollen tube shank shown above. (E) Histogram of LRX8-myc Pdf vs cluster size (blue). Two cluster populations of Gaussian mixture shows mean sizes of 23 nm (monomers 46%) and 59 nm (dimers 54%). 937 clusters were analyzed from 7 pollen tubes from 4 plants. (F) Representative orthogonal projection of Airyscan z-stacks of demethylesterified HG labelled with LM19 in wild-type pollen tubes. Calcofluor white (CFW) signal, mainly staining callose, did not show a patterned distribution. (G) Representative dSTORM image of a wild-type pollen tube labelled with LM19. (H) Histogram of Pdf vs angle, showing two distinct populations of pectin filaments, n=4. (I) Confocal images of sequential immunolabeling targeting *pRALF4::RALF4::HA* in Col-0, and LM19 in pollen tube shanks. Maximal intensity Z-projected image (middle) and pollen tube surface view of X-Z plane (right). (J) (left) Representative pollen tube dSTORM image with immunolabeled *pRALF4:RALF4-HA* and LM19. (right) Bivariate point correlation function (PCF) analysis calculated between RALF4-HA (green) and LM19 (violet) compared to the PCF calculated on randomized data sets. The PCF of experimental data lies above the 95% randomization confidence interval (CI), indicating spatial association between the protein and the polysaccharide.

Fig 3**. LRX8-RALF4-induced pectin compaction promotes cell wall patterning regulating pollen tube growth.**

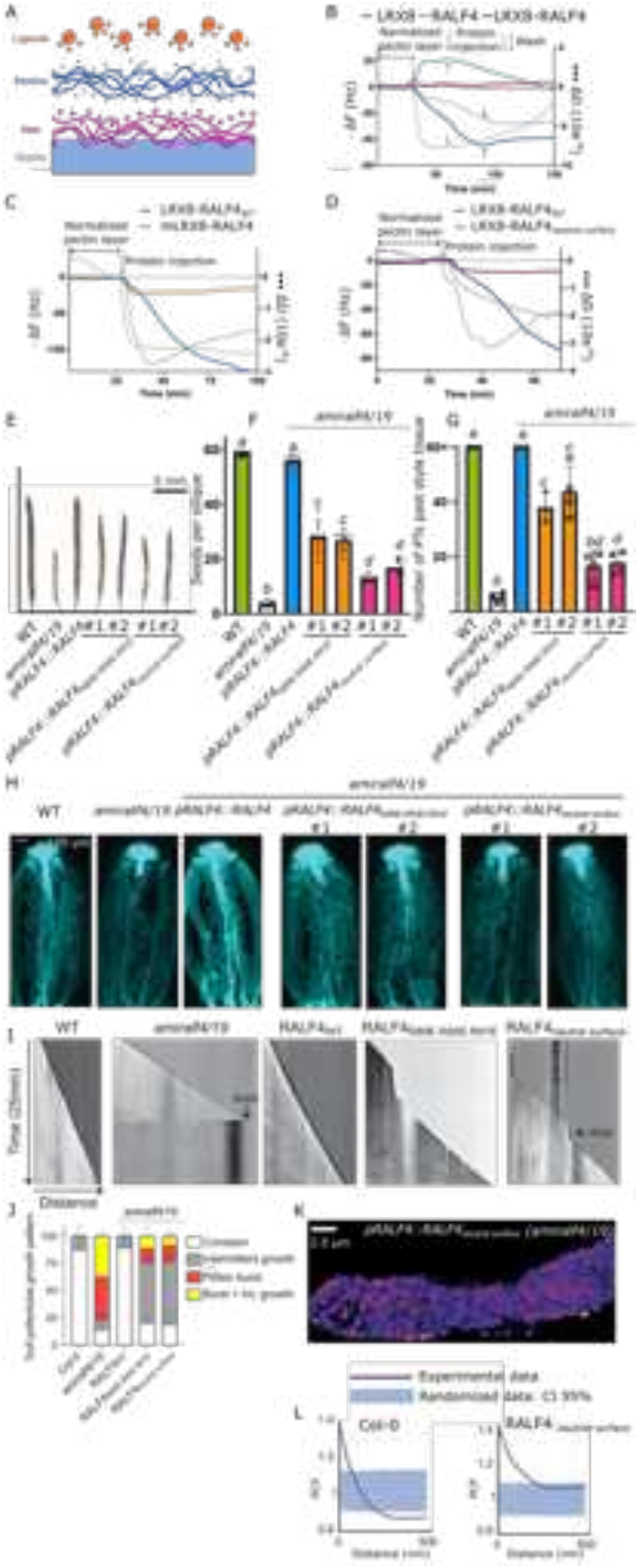

Fig 3**. LRX8-RALF4-induced pectin compaction promotes cell wall patterning regulating pollen tube growth.** (A) Schematic overview of the Quartz Crystal Microbalance with Dissipation monitoring (QCM-D) binding experiments (see fig. S10). (B-D) Representative QCM-D profiles corresponding to the frequency (ΔF, solid lines), and dissipation (ΔD, dotted lines). Protein was injected over a DM43 pectin layer during the period indicated by the arrowheads. (B) QCM-D representative profiles of injecting RALF4 (light blue) (n=7), LRX8-RALF4 (dark blue) (n=16) and LRX8 (pink) (n=3). (C) Representative profiles of dimeric LRX8-RALF4 (blue) (n=16) and monomeric LRX8-RALF4 (orange) (n=3). (D) Representative profiles of LRX8-RALF4 (blue) (n=16), and LRX8-RALF4 $_{\text{neutral surface}}$ (pink) (n=4). (E) and (F) Seeds per silique of Col-0 (WT), *amiralf4/19, pRALF4::RALF4*$_{WT}$, and RALF4 mutants. Error bars are ± SD, n=3. (G) Number of survived pollen tubes past style tissue. Error bars are ± SD, n=3~4. Stat tests = one-way ANOVA ($p<0.0001$) with a multiple comparison using Tukey HSD test. (H) Representative images of pollinated Arabidopsis pistils stained with aniline blue. Pollen from Col-0, *amiralf4/19*, *pRALF4::RALF4*$_{WT}$, and RALF4 mutants were applied to Col-0 stigmas. (I) Representative images of growth kymographs. Arrows indicate either pollen tube bursting or stopping. (J) Quantification of growth patterns from kymographs shown in (I). Error bars are ± SD, 15 pollen tubes per n, n=2. (K) Representative dSTORM image of LM19 on pollen tubes from *amiralf4/19* complemented with *pRALF4::RALF4*$_{neutral\ surface}$. Data is represented as 2D pixelated image (pixel size, 15 nm). (L) Univariate PCF analysis calculated on LM19 dSTORM pointillist data on pollen tubes from Col-0 (left, representative image in Fig. 2G) and *amiralf4/19* complemented with *pRALF4::RALF4*$_{neutral\ surface}$ (right). PCF analysis of the distribution of the LM19 epitope shows that the signal crosses the interval of confidence (CI) in wild-type PTs at shorter distances relative to *pRALF4::RALF4*$_{neutral\ surface}$. This indicates that the LM19 epitope in wild-type PTs, forms densely packed spatially-segregated fibers compared with the *RALF4*$_{neutral\ surface}$ variant.

Fig 4. **LRX-RALF4-pectin patterning is required for cell wall assembly and integrity.**

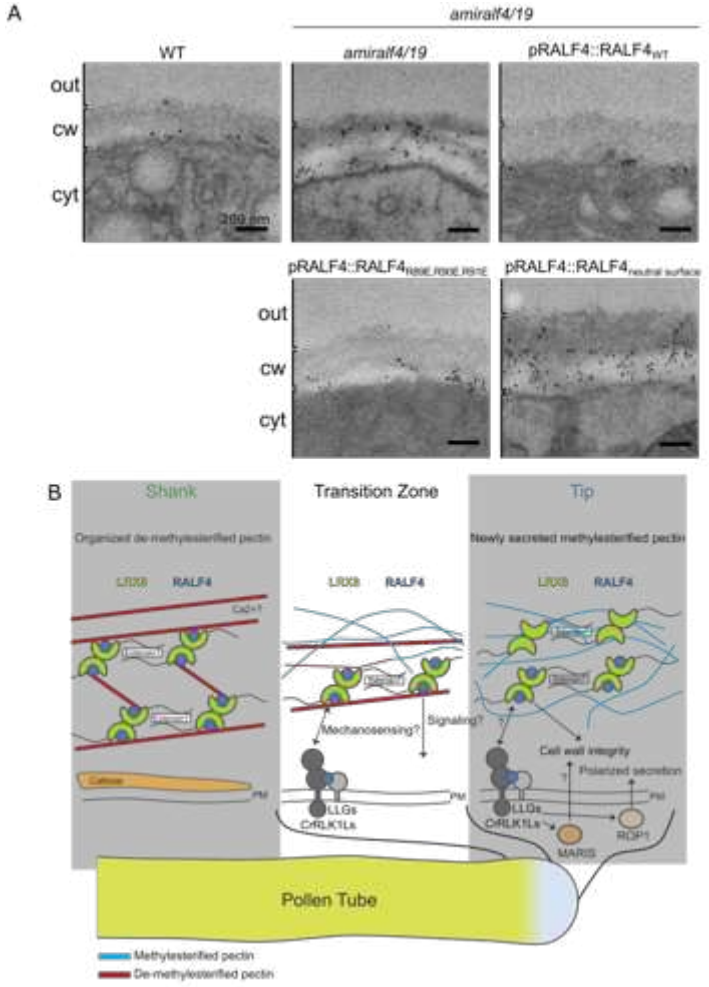

Fig 4. **LRX-RALF4-pectin patterning is required for cell wall assembly and integrity. (**A) RALF4 surface variants display an aberrant cell wall architecture. TEM micrographs of pollen tube transverse sections (~10 μm) of Col-0 (WT), *amiralf4/19,* and complementation lines expressing *pRALF4::RALF4*$_{WT,}$ *pRALF4::RALF4*$_{R89E.R90E.R91E}$ and *pRALF4::RALF4*$_{neutral\ surface}$. Black dots indicate immunogold labelling for callose. Out = outside, cw = cell wall, and cyt = cytoplasm. (B) Proposed molecular model of the two RALF4 activated interacting protein families, to maintain pollen tube cell wall integrity during growth. Methylesterified and demethylesterified pectin are depicted as blue and red lines, respectively. At the tip, membrane spanning *Cr*RLK1Ls and LLGs sense RALF4/19 to activate downstream MARIS and ROP1 proteins to regulate actin dynamics and promote polarized secretion of cell wall components and regulatory proteins. At the transition zone, pectin is shifting to the demethylesterified form via PME activity (*3*) and is then recognized by the LRX-RALF4 complex. The reticulated network of LRX-RALF4 compacts and chaperones the demethylesterified pectin into a criss-crossed filament network. This network contributes to the patterning, reinforcement, and expansion of the cell wall. At the shank, pectin de-methylesterifcation is complete, and the LRX-RALF4-pectin complex remains an integral part of the pollen cell wall. We speculate that the LRX-RALF4-pectin network acts as a load-bearing system during pollen tube expansion, compensating for its low cellulose content. The modularity of the LRX-extensin network, via the binding of different RALF peptides, would allow to target and connect different cell wall polymers or epitopes during cell wall assembly. How the RALF4 membrane and cell-wall systems communicate, how these architectural changes in the cell wall are sensed by the pollen tube cell, and whether the peptide can navigate between the two systems will be interesting topics of future studies.

A

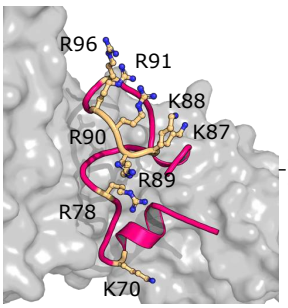

B

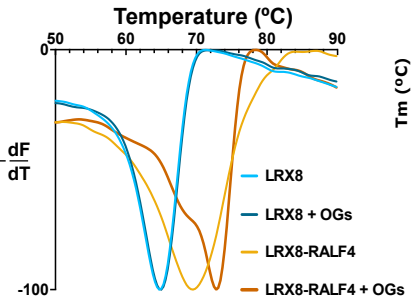

C

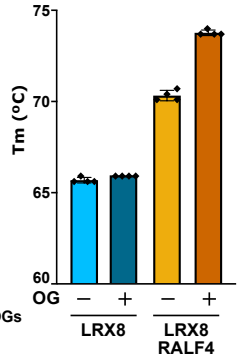

D

		Mock	OGs	Mannuronic Acid	DNA	Sucrose
LRX8	Tm	65.7	65.9	66.2	66.0	66.0
	ΔTm		0.2	0.5	0.3	0.3
LRX8-RALF4	Tm	70.3	73.8	71.2	69.7	69.8
	ΔTm		3.4	0.9	-0.7	-0.5

E

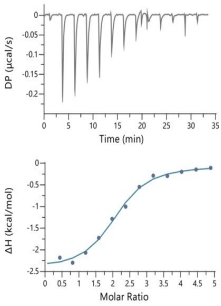

Ligand (syringe)	Protein (cell)	Kd (µM)	ΔH (kcal/mol)	N
OGs	LRX8-RALF4	2 ± 0.5	-2.5 ± 0.1	2
OGs	mLRX8-RALF4	2.9 ± 0.4	-1.8 ± 0.6	1
OGs	LRX8	n.d		
OGs	RALF4	n.d		
OGs	LRX2-RALF4	1.6 ± 0.2	-1.4 ± 0.11	2
DNA	LRX8-RALF4	n.d		

F

		Mock	OG	OG-DM5	OG-DM71
LRX8-RALF4	Tm	68.8	72.7	71.3	69.1
	ΔTm		3.9	2.5	0.3

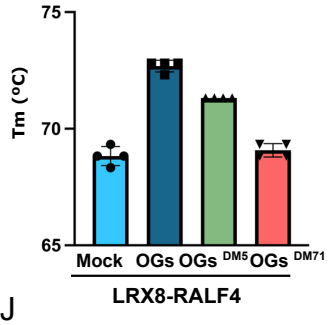

G

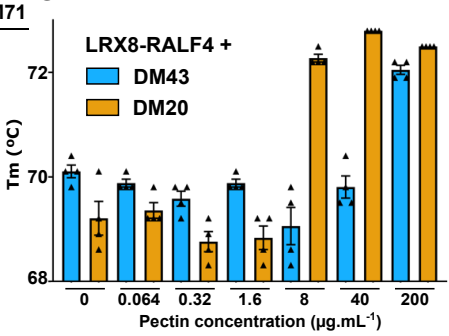

H

Ligand		Pectin concentration (µg/mL) 0	0.064	0.32	1.6	8	40	200
DM43	Tm	69.2	69.9	69.6	69.9	69.1	69.8	72.0
	ΔTm		0.7	0.4	0.7	-0.1	0.6	2.8
DM20	Tm	70.1	69.4	68.8	68.8	72.3	72.8	72.5
	ΔTm		-0.7	-1.3	-1.3	2.2	2.7	2.4

J

LRX8-RALF4 $_{\text{neutral surface}}$ vs OGs

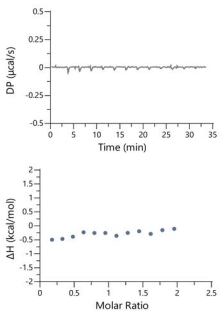

I

		LRX8-RALF4$_{R89E.R90E.R91E}$	LRX8-RALF4$_{\text{neutral surface}}$
Mock	Tm	73.7	73.4
	Tm	74.6	72.1
		0.9	**-1.3**

Ligand (syringe)	Protein (cell)	Kd (µM)	ΔH (kcal/mol)	N
OGs	LRX8-RALF4$_{R89E.R90E.R91E}$	8.5 ± 0.4	-5.6 ± 1.6	2
OGs	LRX8-RALF4$_{\text{neutral surface}}$	n.d.		

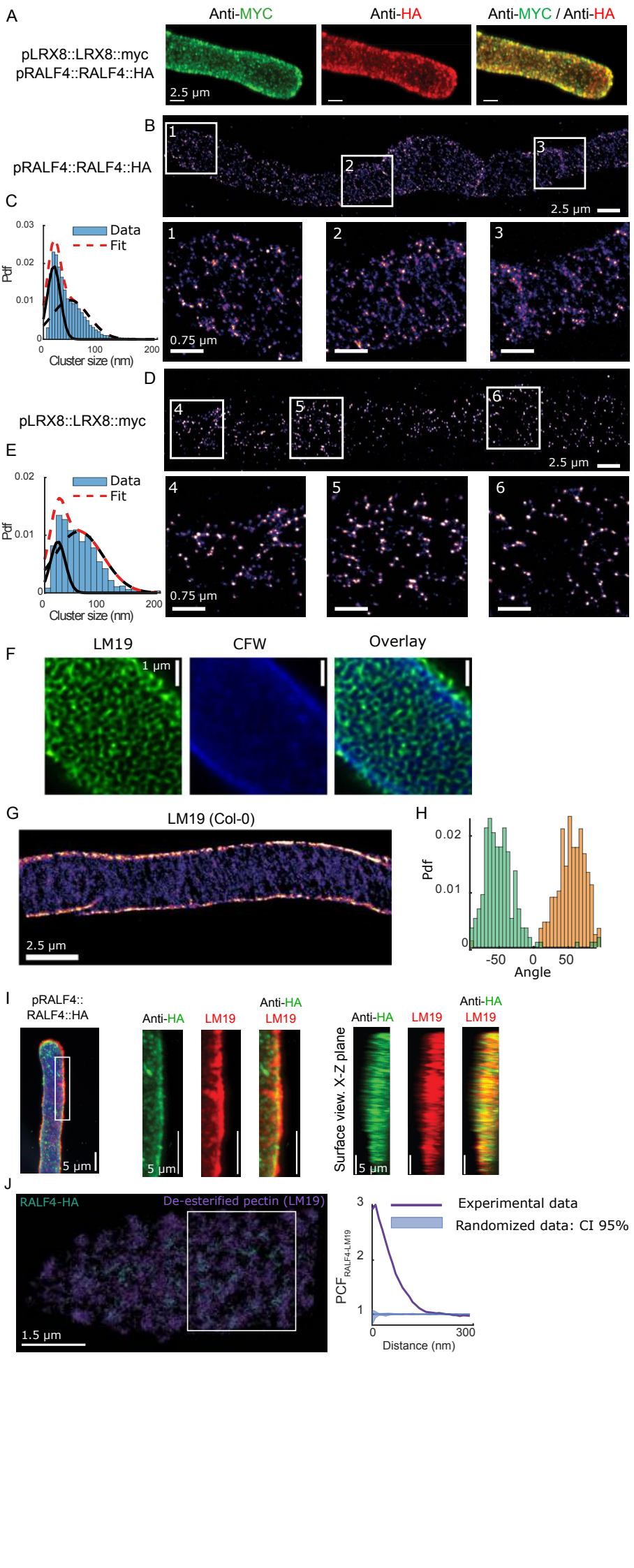
A
Anti-MYC
Anti-HA
Anti-MYC / Anti-HA
pLRX8::LRX8::myc
pRALF4::RALF4::HA
2.5 µm
B
pRALF4::RALF4::HA
1
2
3
2.5 µm
C
Data
Fit
Pdf
Cluster size (nm)
0.75 µm
D
pLRX8::LRX8::myc
4
5
6
2.5 µm
E
Data
Fit
Pdf
Cluster size (nm)
0.75 µm
F
LM19
CFW
Overlay
1 µm
G
LM19 (Col-0)
2.5 µm
H
Pdf
Angle
I
pRALF4::
RALF4::HA
Anti-HA
LM19
Anti-HA
LM19
Surface view. X-Z plane
5 µm
J
RALF4-HA
De-esterified pectin (LM19)
1.5 µm
Experimental data
Randomized data: CI 95%
PCF RALF4-LM19
Distance (nm)

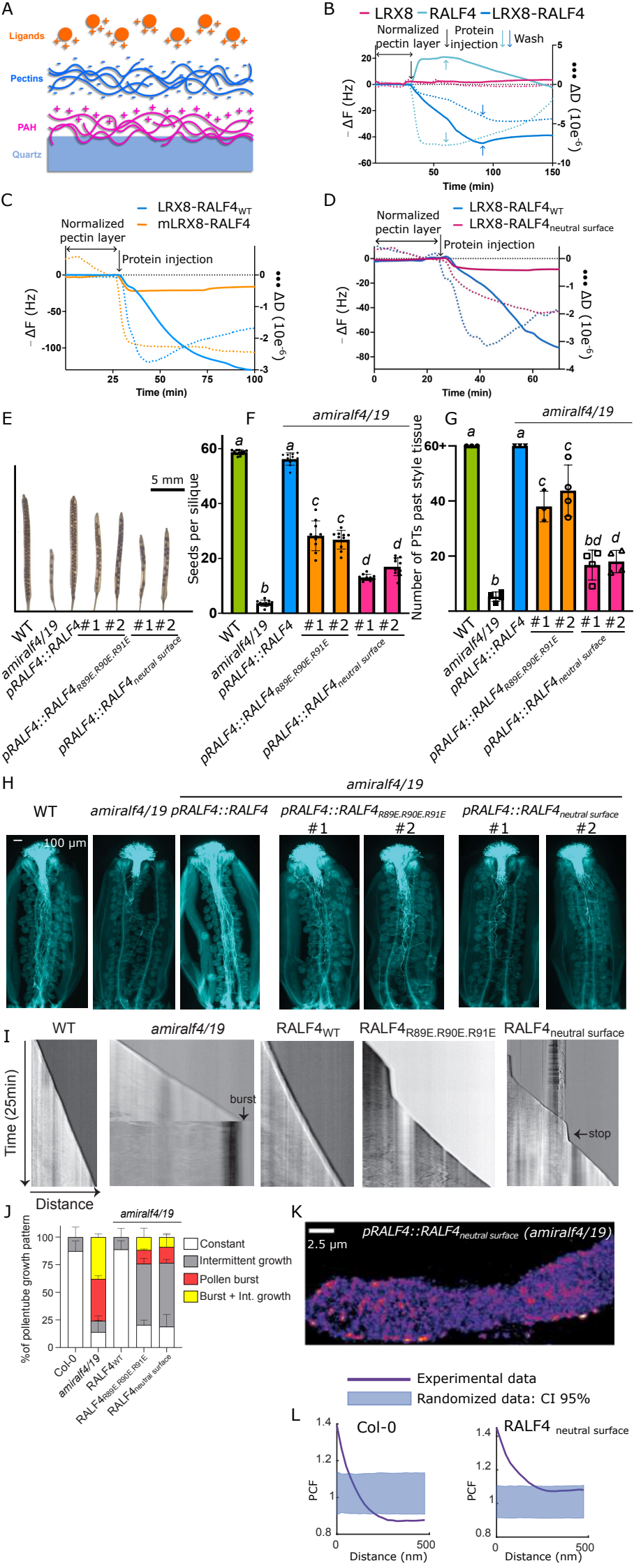
A
Ligands
Pectins
PAH
Quartz
B
LRX8
RALF4
LRX8-RALF4
Normalized pectin layer
Protein injection
Wash
−ΔF (Hz)
ΔD (10e-6)
Time (min)
C
LRX8-RALF4WT
mLRX8-RALF4
Normalized pectin layer
Protein injection
−ΔF (Hz)
ΔD (10e-6)
Time (min)
D
LRX8-RALF4WT
LRX8-RALF4neutral surface
Normalized pectin layer
Protein injection
−ΔF (Hz)
ΔD (10e-6)
Time (min)
E
5 mm
WT
amiralf4/19
pRALF4::RALF4
pRALF4::RALF4R89E.R90E.R91E
pRALF4::RALF4neutral surface
#1 #2
#1#2
F
amiralf4/19
Seeds per silique
G
amiralf4/19
Number of PTs past style tissue
H
amiralf4/19
WT
amiralf4/19
pRALF4::RALF4
pRALF4::RALF4R89E.R90E.R91E
pRALF4::RALF4neutral surface
#1
#2
100 µm
I
WT
amiralf4/19
RALF4WT
RALF4R89E.R90E.R91E
RALF4neutral surface
Time (25min)
Distance
burst
stop
J
amiralf4/19
%of pollentube growth pattern
Constant
Intermittent growth
Pollen burst
Burst + Int. growth
Col-0
amiralf4/19
RALF4WT
RALF4R89E.R90E.R91E
RALF4neutral surface
K
2.5 µm
pRALF4::RALF4neutral surface (amiralf4/19)
Experimental data
Randomized data: CI 95%
L
Col-0
RALF4 neutral surface
PCF
Distance (nm)

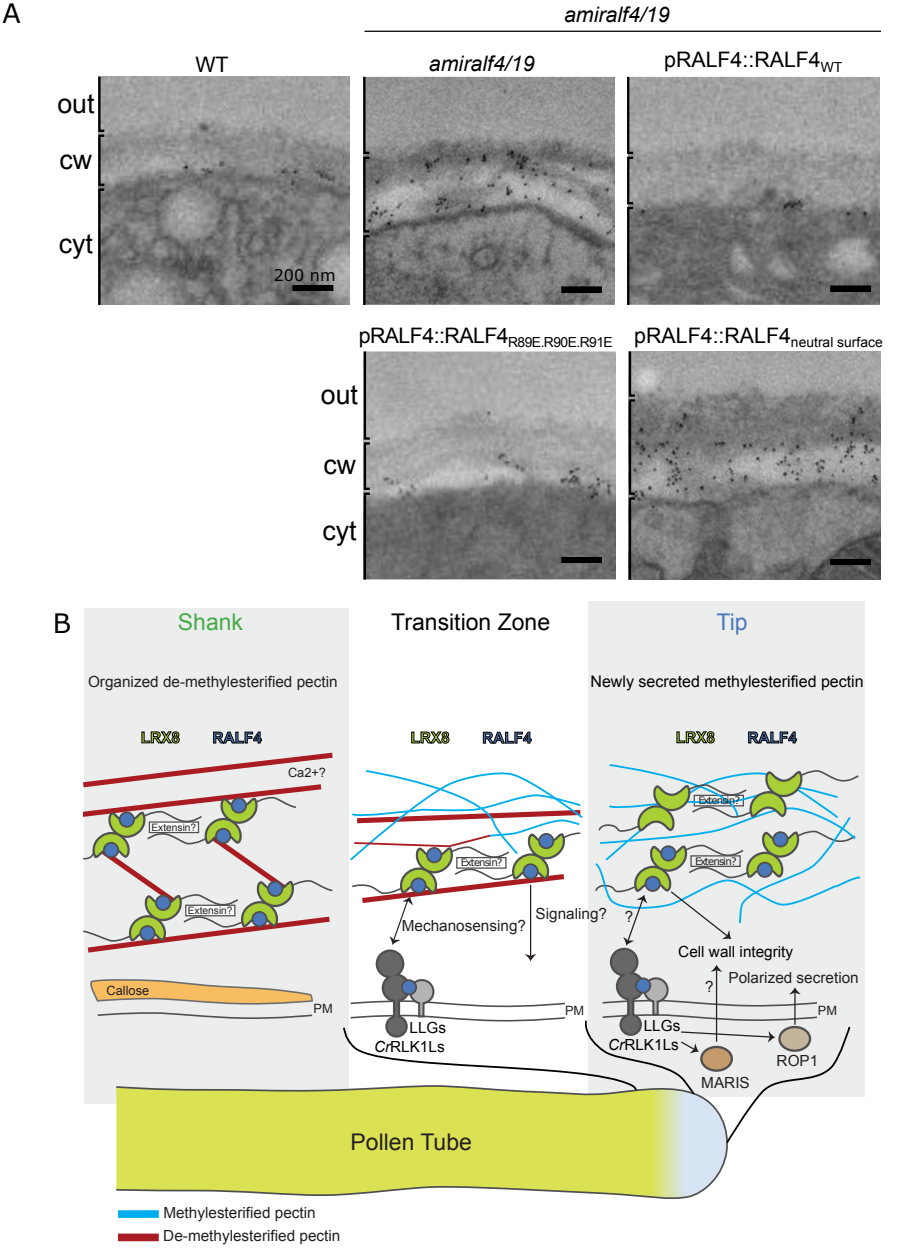
A
amiralf4/19
WT
amiralf4/19
pRALF4::RALF4WT
out
cw
cyt
200 nm
pRALF4::RALF4R89E.R90E.R91E
pRALF4::RALF4neutral surface
B
Shank
Transition Zone
Tip
Organized de-methylesterified pectin
Newly secreted methylesterified pectin
LRX8
RALF4
Ca2+?
Extensin?
Callose
PM
Mechanosensing?
Signaling?
LLGs
CrRLK1Ls
Cell wall integrity
Polarized secretion
MARIS
ROP1
Pollen Tube
Methylesterified pectin
De-methylesterified pectin

Science
AAAS

Supplementary Materials for

Plant cell wall patterning and expansion mediated by receptor-peptide-polysaccharide interaction.

Steven Moussu[1†‡], Hyun Kyung Lee[1†], Kalina T. Haas[2], Caroline Broyart[1], Ursina Rathgeb,[3] Damien De Bellis[4,3], Thomas Levasseur[5], Sébastjen Schoenaers[2,6], Gorka S. Fernandez[7], Ueli Grossniklaus[7], Estelle Bonnin[5], Eric Hosy[8], Kris Vissenberg[6,9], Niko Geldner[3], Bernard Cathala[5], Herman Höfte[2]*, Julia Santiago[1]*

[1]The Plant Signaling Mechanisms Laboratory, Department of Plant Molecular Biology, University of Lausanne, 1015, Lausanne, Switzerland.

[2]Université Paris-Saclay, INRAE, AgroParisTech, Institut Jean-Pierre Bourgin (IJPB), 78000, Versailles, France.

[3]Department of Plant Molecular Biology, University of Lausanne, 1015 Lausanne, Switzerland.

[4]Electron Microscopy Facility, University of Lausanne, Lausanne, Switzerland.

[5] INRAE, UR1268 BIA, F-44300 Nantes, France.

[6]Integrated Molecular Plant Physiology Research (IMPRES), Department of Biology, University of Antwerp, Groenenborgerlaan 171, 2020 Antwerp, Belgium.

[7]Department of Plant and Microbial Biology & Zurich-Basel Plant Science Center, University of Zurich, 8008 Zurich, Switzerland.

[8]IINS, CNRS UMR5297, University of Bordeaux, 33000 Bordeaux, France

[9]Plant Biochemistry & Biotechnology Lab, Department of Agriculture, Hellenic Mediterranean University, Stavromenos PC 71410, Heraklion, Crete, Greece

[†] These authors contributed equally to this work

*Corresponding authors. Emails: hermanus.hofte@inrae.fr, julia.santiago@unil.ch

‡

[‡] Present address : Laboratoire de Recherche en Sciences Végétales, Université de Toulouse, CNRS, UPS, Toulouse INP, 31320 Auzeville Tolosane, France.

This PDF file includes:

Materials and Methods

Figs. S1 to S18

References (*55–63)*

Materials and Methods

Protein expression and purification

Spodoptera frugiperda codon-optimized synthetic genes (Invitrogen GeneArt), coding for *Arabidopsis thaliana* LRX8 (residues 49 to 400; At3g19020), LRX2 (residues 1 to 385; At1g62440), LLG3 (residues 24 to 137; At4g28280), RALF4 wild-type (residues 48 to 110; At1g28270) and RALF4 mutants were cloned into a modified pFastBAC vector (Geneva Biotech) providing a 30K signal peptide (*55*), a N- or C-terminal TEV (tobacco etch virus protease) cleavage site, and a StrepII-9xHis affinity tag. $RALF4_{WT}$ and RALF4 mutants were fused to a TRX A (Thioredoxin A) to favor disulfide bond formation. Baculovirus generation was carried out using DH10 cells and virus production and amplification was done in Sf9 cells. *Trichoplusia ni* Tnao38 cells (*56*) were used for protein expression: they were infected with LLG3 or co-infected with LRX8-RALF4 or LRX2-RALF4 viruses with a multiplicity of infection (MOI) of 3 and incubated 1 day at 28°C and 2 days at 22°C at 110 r.p.m. The secreted proteins and complexes were purified on Ni^{2+} (HisTrap excel, Cytiva, equilibrated in 25 mM KP_i pH 7.8 and 500 mM NaCl) followed by Strep affinity chromatography (Strep-Tactin Superflow high-capacity, IBA Lifesciences, equilibrated in 25 mM Tris pH 8.0, 250 mM NaCl, 1 mM EDTA) affinity chromatography. All proteins were incubated with TEV protease to remove the tags and fused proteins. Proteins were further purified by SEC on a Superdex 200 Increase 10/300 GL column (Cytiva) equilibrated in 20 mM citrate pH 5.0, 150 mM NaCl. LRX8 and RALF4 proteins were obtained by complex dissociation in a SEC column equilibrated in 20 mM citrate pH2.0, 150 mM NaCl followed by dialysis against 20 mM citrate pH 5.0, 150 mM NaCl as described in Moussu *et al*. (*10*). Proteins were concentrated using Amicon Ultra concentrators (Millipore, molecular weight cut-off 3,000, 10,000 and 30,000), and SDS-PAGE was used to assess the purity and structural integrity of the different proteins.

Preparation of partially methylated OGs and Homogalacturonan

High methoxy (HM) and low methoxy (LM) citrus pectin kindly provided by C.P. Kelco, were used as starting material to produce HM, LM and demethoxylated homogalacturonan (HG), as well as oligosaccharides. The preparation of HM and LM HGs consists of subjecting pectin of high and low DM respectively to a combination of enzymes allowing the degradation of rhamnogalacturonans and their side chains. The protocol used was described in Bonnin et al. (*57*), except for the use of pectin methylesterases to keep the methyl groups in their initial number and position. HM or LM pectin (200 mg) were solubilized

in 50 mM succinate buffer pH 4.5 (25 mL). A mixture containing 5 nkat of rhamnogalacturonan-hydrolase (Novozyme) + 100 nkat endo-galactanase (E-GALN, Megazyme) + 100 nkat endo-arabinanase (E-EARAB, Megazyme) + 50 nkat arabinofuranosidase (E-AFASE, Megazyme) was added. The reaction medium was incubated overnight on a wheel at 40°C. The reaction was then stopped by boiling and the solution was concentrated. HG was precipitated by adding ethanol. The precipitate was recovered by centrifugation, successively washed with water and ethanol, and finally dried by solvent exchange.

Methylated oligosaccharides ($OGs^{DM5\ and\ DM71}$) : autolysis of demethoxylated HG at 100°C allowed the production of oligosaccharides with various degrees of polymerization. After precipitation in ethanol 35%, the soluble fraction contained oligosaccharides with a degree of polymerization centered on 12. It was dialyzed against water to remove minor amounts of monomers and dimers. The oligosaccharides were freeze-dried, suspended in dimethyl sulfoxide and further fully methylated by adding iodomethane CH3I. A controlled de-esterification with sodium hydroxide was finally performed overnight at 4°C to reach the targeted degrees of methylation.

Thermal Shift Assay

Thermal shift assays (TSA) were performed as described in (*58*). Samples were prepared in a final volume of 30 µL with the following composition: Proteins were diluted to a concentration of 5 µM in 20 mM Na-Acetate, 20 mM NaCl, pH 5.5. The usual concentration of ligand was 100 µM or otherwise indicated in the figure. SYPRO Orange (Molecular Probes, CA) fluorescent probe was used at a 5X concentration. Samples were loaded in MicroAmp™ Fast 96-Well Reaction Plates (0.1 mL, Applied Biosystems; Thermo Scientific) and sealed with MicroAmp™ Optical Adhesive Film (Applied Biosystems; Thermo Scientific). Plates were then inserted in a QuantStudio three real-time PCR machine (Applied Biosystems; Thermo Scientific) to run the assay. The temperature was increased at a rate of 0.5°C per minute between 30°C and 90°C. The fluorescence at 530 nm was recorded every minute. The negative of the derivative of the fluorescence (F) as a function of the temperature (T) (-dF/dT) was plotted, and the minima was used to determine the T_m. Graphs were plotted using Prism 9 (GraphPad Software, LLC). Number of technical replicates n=4 and experiments were performed at least 3 independent times.

Ligands used during the experiments: 14-mer oligo DNA (GAT TAC AGA TTA CA), D-(+)-Galacturonic Acid Monohydrate (Sigma Aldrich, 48280), Digalacturonic Acid (Sigma Aldrich, D4288), OGs DP10-15 (Elicityl, GAT114), OGs DP 3-4 (Elicityl, GAT111), OGs DP5-7 (Elicityl, GAT11x), Polymannuronic acid (Average MW < 5000 Da, YP03136, Carbosynth), D-(+)- Saccharose (4621.1, Carl Roth).

Isothermal titration calorimetry (ITC)

Experiments were performed at 25 °C using a MicroCal PEAQ-ITC (Malvern Instruments) with a 200 µL standard cell and a 40 µL titration syringe. Proteins were either dialyzed against the corresponding ITC buffers (20 mM citrate pH 5.0, 150 mM NaCl or 20 mM HEPES pH 7.5, 150 mM NaCl), or desalted (PD-10 desalting column, Cytiva) in 20 mM Na-Acetate pH 5.5, 20 mM NaCl when used in the binding experiments with pectins. The LRX8-RALF4 *vs*. OGs DP10-15 (Elicityl, GAT114) and 14-mer DNA (GAT TAC AGA TTA CA) oligo experiments were performed using a 50 µM protein solution in the cell and 500 µM of the ligand in the syringe. The concentration of potential active ligand molecules was calculated based on TSA assays (Fig. S1A) and HPLC results of the OG mixed (Fig.S1E.), and estimated to be from DP6. A typical experiment consisted of injecting 3 µl of ligand solution into the cell at 150 s intervals and 500 r.p.m stirring speed. In the case of LRX8 vs. RALF4 mutants, interactions were measured in 20 mM citrate pH 5.0, 150 mM NaCl and performed with 10 µM of LRX8 in the cell and 100 µM of RALF4 peptides in the syringe using similar intervals and stirring speed. LLG3 vs. RALF4 mutant interactions were performed in 20 mM HEPES pH 7.5, 150 mM NaCl. ITC data were corrected for the heat of dilution by subtracting the mixing enthalpies for titrant solution injections into protein free ITC buffer. Experiments were done in duplicates or triplicates, and data were analyzed using the MicroCal PEAQ-ITC Analysis Software provided by the manufacturer.

Analytical size-exclusion (SEC) chromatography

Analytical SEC experiments were performed using a Superdex 200 Increase 10/300 GL column (Cytiva). The columns were pre-equilibrated in 20 mM citric acid pH 5, 150 mM NaCl. 150 µg of LRX8-RALF4 and the different mutant variants were injected sequentially onto the column and eluted at 0.5 mL/min. Ultraviolet absorbance (UV) at 280 nm was used to monitor the elution of the proteins. The peak fractions were analyzed by SDS-PAGE followed by Coomassie blue staining.

QCM-D (Quartz Crystal Microbalance with Dissipation Monitoring)

Quartz Crystal Microbalance with Dissipation Monitoring (QCM-D) was used to evaluate, for RALF4, LRX8, LRX8-RALF4 and LRX8-RALF4 variants, the association with pectin layers of different degrees of methylesterification and the rheological effects of this association on the pectin layer. All QCM-D runs were carried out with a "Q-Sense Analyser" from Biolin Scientific (Gothenburg, Sweden) using gold-

coated SiO_2 base sensors (QSX 301), spin-coated with 1% polyallylamine hydrochloride (PAH, Sigma-Aldrich, product number 283223) dissolved in water. A continuous flow of 0.1% (w/w) pectin was coupled to the PAH layer in a sodium acetate buffer (10 mM Na-Acetate pH 5.6, 10 mM NaCl). After a washing step with buffer to remove the excess of uncoupled pectin, the indicated protein in each experiment at a concentration of 1 µg/ml (free RALF4) or 10 µg/ml (LRX8, LRX8-RALF4 and LRX8-RALF4 variants), was flown over the pectin layer, followed by a washing step. Protein solutions were continuously supplied from the start to the end of the boxed area. Data presented are frequency (ΔF) and dissipation rate (ΔD) of the 3rd harmonic resonant frequency of the base gold-coated sensors and individual data sets are representative for at least three independent experiments. Before reutilization, sensors were cleaned with a "Piranha" solution (7 vol 95% H_2SO_4 added to 3 vol 30% H_2O_2; respect the order!) using the following protocol: the quartz was incubated (4 in a holder) for 3-5 min in Piranha solution. Next, the holder with quartz was moved to two successive baths with MilliQ water. Then, each quartz was individually rinsed with MilliQ water and dried under a nitrogen stream. If traces still appeared on the surface during drying, the rinsing and drying steps were repeated.

Plant material and generation of transgenic lines

Plants were grown in long days (16 h day, 8 h dark, 22˚C). All transgenic lines used in this study were built in the Columbia-0 (Col-0) accession. The *ppme1* mutant (SALK_077776C) and *amiralf4/19* line were described in Tian *et al.* (*34*) and Mecchia *et al*. (*9*), respectively. For complementation assays using mutated versions of RALF4, plasmids containing *pRALF4::rRALF4*$_{WT}$, *pRALF4::rRALF4*$_{R89E.R90E.R91E}$, *pRALF4::rRALF4*$_{neutral\ surface}$, were generated by altering the sequence of rRALF4 (amiRNA resistant), as reported in Mecchia *et al*. (*9*). The RALF4 promoter was amplified using the following primers: Fw-5': TGA ATT CAA AAT AGT GAA ATT ATT AAC AT, Rv-5': TAA GAA CAA ATG AGA GAT TGG TTT TGT TG. The following reporter lines were made using the 3XHA tag: *pRALF4::rRALF4*$_{WT}$*::HA*, *pRALF4::rRALF4*$_{neutral\ surface}$*::HA, and pRALF4::rRALF4*$_{R89E.R90E.R91E}$*::HA*. All plasmids were transformed in *Agrobacterium tumefaciens*, and plants were consequently transformed using the floral dip method. For the complementation lines, expression of the correctly mutated rRALF4 versions were analyzed by pollen RNA extraction, RT-PCR and sequencing of the amplified RALF4 variants. *ppme1* mutants were genotyped using the following primers: *ppme1_LP*: CCG ATA TTG AGG CTC AGA ATG, *ppme1_RP* : TTA ACG GCC ATG AAA TAG TCG and *LBb1.3* : ATA TTG ACC ATC ATA CTC ATT GC.

Aniline blue staining and pollen tube counts

Aniline blue assays used manual pollinations and were conducted with slight modification as described in (*59*). To manually pollinate Col-0 pistils with Col-0, pRALF4:RALF4 or RALF4 mutant pollen grains, stage 12 flower buds (*60*) were emasculated and wrapped in plastic wrap. All aniline blue experiments were done on T3 generations of transgenic lines. At 24-hours post-emasculation, pistils with fully elongated papillae were lightly pollinated using a single anther per pistil of Col-0, pRALF4::RALF4 or pRALF4::RALF4 mutants. At 24-hours post-pollination, the pistils were submerged in 300 µL fixative (3:1 ethanol: glacial acetic acid) at room temperature (RT) for at least 30 min. After incubation, pistils were then submerged in 8 M NaOH overnight at RT, followed by a series of three washes with 500 µL of sterile water. Finally, pistils were stained with 500 µL of 0.1% (w/v) aniline blue at 4°C overnight and was mounted on a slide with water. Aniline blue images were taken using a Leica Thunder Imager fluorescence microscope. With the captured aniline blue images, a dotted line was drawn on the junction between the transmitting tract and the style tissue. Then, the pollen tube emerging from the style into the transmitting tract, thus experiencing a sudden pressure change, were counted. Pollen tubes were counted until 60, which is approximately the maximum number of ovules.

Seed counts, pollen growth assays, and kymographs

For each line, 10 browning siliques per plants were harvested, with n=4 individual plants per line. Siliques were cleared at RT for 24h in EtOH 70%. Seeds were counted by siliques using the Cell Counter plugin in Fiji (n=10). Statistical analysis was performed with Prism 9, using and two-way ANOVA followed by multiple comparisons using Tukey HSD tests. Pollen was germinated in solid germination medium (0.01% boric acid [wt/vol], 5 mM $CaCl_2$, 5 mM KCl, 1 mM $MgSO_4$, 10% sucrose, pH 7.5, Low melting agarose 1.5%). Standard microscopy slides were covered with 450 µL of solid medium. Upon media solidification, pollen was harvested from freshly opened flower by gently tapping them onto agar-covered slides. Slides covered in pollen were incubated in a moist chamber for 2-3 h prior to imaging. A total of 100 µL of liquid germination media, without agar, was then applied onto the pollens, and covered with a coverslip. For speed monitoring, images were taken at 10 min interval using a Leica Thunder microscope and analyzed using Fiji. For the generation of kymograph, images were taken at 5 second intervals for 25 minutes using a Leica Thunder Imager microscope and analyzed using Fiji.

Immunostaining, confocal and Airyscan microscopy image acquisition, and data processing

For histoimmuno chemistry, pollen tubes were grown semi in vivo for 3 h as described in Fabrice *et al*., 2018 *(33)* in glass bottom petri dishes. After germination, pollen tubes were fixed for 15 min in Phosphate-Buffer Saline (PBS) + Paraformaldehyde (PFA) 3.5%, then washed with PBS 3x5 min. Remaining PFA was quenched using 100 mM NH_4Cl in PBS and rinsed 3x5 min with PBS. Fixed pollen tubes were then blocked in PBS + Milk 5% or BSA 3% at RT for 2 h. Incubation in primary antibodies, diluted in PBS + BSA 3%, was then directly performed at RT for 2 h or at 4°C overnight, (LM19/LM20 Rat IgM dilution 1:50, anti-HA mouse IgG dilution 1:100, anti-MYC mouse IgG dilution 1:100), and washed 3x5 min in PBS. Secondary antibody incubation was then performed in PBS + BSA 3% at RT for 2h. Samples were then washed 3x5 min in PBS. Finally, samples were counterstained using Fluorescent Brightener 28 disodium salt solution (Sigma-Aldrich, 910090-20ML), diluted 1:200 in PBS, for 10 min at RT, and then subsequently washed 3x5min. For sequential staining using two mouse antibodies, samples were subjected to the same protocol a second time, starting at the fixation step to immobilize the first staining procedure. Individual pistils were then mounted in CitiFluor™ AF1 mounting medium between a slide and a cover-slide. Pollen tubes were then imaged using a Leica Stellaris 5.

Airyscan images were acquired with a 90° flipped confocal laser scanning microscope ZEISS LSM980 equipped with an Airyscan 2 detection unit. All images were acquired with a Plan-Apochromat 63X/1.40 Oil DIC M27 objective. Immersion oil Immersol 518 F (ne =1.518 (23 ◦C); Carl Zeiss) was used during image acquisition. All pictures were acquired in Airyscan-SR mode. Microscope settings were as follows: Zoom: 8.4x, detector gain: 700, pixel dwell time: 1.16 µs, bidirectional scanning, Scan Mode: Frame. Laser settings: 405 nm - 0.2% (Calcofluor White), 488 nm - 0.4% (LM19-AlexaFluor488). Z-stacks were acquired to visualize the lattice shaped distribution of LM19-AlexaFluor488 at the apical shank of the pollen tube by acquiring 44 individual z-slices with a distance of 0.15 µm covering total of 6.5 µm.

Zen Blue 3.4 software was used to process the raw Airyscan dataset, which processed images 32 detector elements, shifts and sums the signal. Images were processed by joint deconvolution (jDCV) algorithm developed by Zeiss. Raw Airyscan datasets were processed by Dr. Christine Strasser courtesy of Zeiss Switzerland. As deconvolution strength 20-iterations were chosen in order to enhance spatial resolution and to avoid artefacts from over-processing. Images are representing orthogonal projections of all 44

individual z-slices. Brightness was adjusted in order to enhance visibility of the lattice structure visible as LM19-Alexafluor488 signal. Antibody information:

Anti-HA (RRID:AB_444303, Supplier: Abcam, Catalogue number: AB18181-1001).

Anti-MYC (RRID: AB_10895876, Supplier: Sigma, Catalogue number: SAB4700447).

LM19 (Supplier: Megazyme, Catalogue number: AB-LM19).

LM20 (Supplier: Megazyme, Catalogue number: AB-LM20).

Alexa Fluor plus 488 goat anti-rat (RRID: AB_2896330, Supplier: Thermo, Catalogue number: A48262).

Anti-Rat IgG CF680 (Supplier: Sigma, Catalogue number: SAB4600201).

Anti-Mouse IgG Atto488 (RRID: AB_1137649, Supplier: Sigma, Catalogue number: 62197-1mL-F).

Anti-Mouse IgG CF568 (Supplier: Sigma, Catalogue number: SAB4600082).

Alexa Fluor 647 goat anti-rat IgG (RRID: AB141778, Supplier: Thermo, Catalogue number: A21247).

Electron microscopy

Arabidopsis pollen tubes were prepared as described in Fabrice et al., 2018 (*44*). Arabidopsis pollen tubes were grown semi *in vivo* for 3 h in pollen germination media in glass bottom petri dishes. Pollen tubes were fixed in a mixture of 2.5% glutaraldehyde (EMS, Hatfield, PA), 1% osmium tetroxide (EMS, Hatfield, PA, USA), and 1.5% of potassium ferrocyanide (Sigma, St. Louis, MO, USA) in PB buffer for 1 h at RT. The samples were then washed several times in distilled water and dehydrated in acetone solution (Sigma, St Louis, MO, US) at graded concentrations (30%-15 min; 50% - 15 min; 70% - 15 min; 100% - 3x20 min). This was followed by infiltration in Epon resin (EMS, Hatfield, PA, USA) at graded concentrations (Epon 33% in acetone, 45 min; Epon 66% in acetone, 45 min; Epon 100%-12 h). Then the samples were mounted within a thin layer of Epon resin between two aclar film (EMS, Hatfield, PA, USA) and finally polymerized for 48 h at 60°C in an oven. Ultrathin sections of 50 nm thick were cut transversally 5-10 µm and 20-25 µm below the pollen tube tip, using a Leica UC7 (Leica Mikrosysteme GmbH, Vienna, Austria), and picked up on a copper slot grid of 2x1 mm (EMS, Hatfield, PA, USA) coated with a polystyrene film (Sigma, St Louis, MO, USA). To precisely target the right position of the pollen tube, the Keyence VHX-7000 digital microscope (Keyence International, Mechelen, Belgium) was used to measure the distance from the tip of the tube. Micrographs were taken with a transmission electron microscope FEI CM100 (FEI, Eindhoven, The Netherlands) at an acceleration voltage of 80 kV with a TVIPS TemCamF416 digital camera (TVIPS GmbH, Gauting, Germany) using the software EM-MENU 4.0 (TVIPS GmbH, Gauting, Germany).

To target the callose localization, immunogold labeling against (1→3)-β-Glucan was performed. Ultrathin sections were first incubated in 50 mM ammonium chloride (Sigma) solution for 10 min to block aldehydes. Then, sections were incubated in the blocking solution for donkey gold conjugate (Aurion) for 1 h to inhibit nonspecific binding of antibodies. Afterwards, sections were incubated with the primary mouse monoclonal antibody (IgG) against (1→3)-β-Glucan (Biosupplies Australia), diluted 1:20 in 0.1% BSAc in PBS (PBS; 0.15 M, pH 7.4; Sigma) for 1 h at room temperature. Sections were washed six times in 0.1% BSAc in PBS, and then incubated with the secondary antibody (6-nm Gold particles, Donkey Anti-Mouse IgG; Aurion) in 1:40 dilution in 0.1% BSAc in PBS for 1 h at RT. Sections were then washed four times in 0.1% BSAc in PBS, followed by another four times in PBS, and a last washing step of ten times in water.

STORM microscopy

Pollen tubes were prepared similarly as for immunostainings. After coupling with primary and secondary antibodies, instead of counterstaining with calcofluor white, to prevent thermal drift of antibodies pollen tubes were post-fixed for 15 min in 3.5% PFA in PBS and washed 3x5 min in PBS. For imaging, pistils with pollen tubes were deposited on cover slides functionalized with 3% triethoxysilane in ddH_20 for 15 min, and rinsed twice in ddH_20 for 5 min and left to dry. Pistil-attached pollen tubes were then gently deposited on the slide, and PBS was replaced with the OxEA dSSTORM imaging buffer (*61*, *62*) containing: 50-100 mM MEA-HCL (Sigma, M6500), 3% (v/v) OxyFlour™ (Oxyrase Inc., Bioquote, OF-0005), 20% (v/v) sodium DL-lactate solution (L1375, Sigma) in final 1X PBS buffer at pH 8.5.

Direct Stochastic Optical Reconstruction Microscopy (d-STORM)

Samples were imaged at RT in an open Attofluor (Fisher Scientific, A7816) chamber with the 25 mm glass-bottom coverslips on an inverted Nikon TiU2 Microscope or DMI8 Leica microscope. Samples were imaged in highly inclined illumination mode using Apochromat 100x/1.49 NA oil immersion objective. Both microscopes were equipped with Abbelight's SAFE360imaging system and operated by NEO software. Typically~30,000 frames were acquired using a Hamamatsu's sCMOS Orca Flash BT camera with ~20 ms frame acquisition time. CF680 dye was imaged with 640 nm, and CF568 with 561 nm excitation laser line.

dSTORM data analysis

The single molecule localization was performed with Abbelight NEO software. For further analysis, the molecular localization lists from NEO software were imported to custom-written Matlab-based single-molecule data analysis software (*27*, *62*, *63*). Two-point correlation function (PCF) and nearest neighbour distance (NND) analysis was performed on the 'pointilist' dSTORM data using Grafeo software as previously described in Peaucelle *et al*., and Haas *et al*. (*62*, *63*). Shortly, PCF and NND are the spatial statistics functions that can evaluate the spatial arrangement of different epitopes. Bivariate PCF estimates the number of type 1 molecule within a thin ring centered at the type 2 molecule, normalized to the expected number under the independent distribution. The empirical PCF was compared with the randomized PCF, calculated by the repetitive random reallocation of the experimental points. Randomized distributions have the average PCF=1, indicating spatial independence between two epitopes. If the experimental PCF lies above the 95% confidence interval (CI, blue shaded area) at a given distance, it suggests a spatial association, and below 5% CI, it suggests segregation.

Fiber orientation analysis was performed using custom written Matlab routine. Fibers were detected using morphological operations using the Matlab bwmorph function with arguments ('thin', inf) to skeletonize fibers, and'branchpoints' to find branchpoints to separate crossing fibers. The orientation was calculated using the regionprops function with the argument 'orientation' that is reporting the angle between x-axis and the major axis of an ellipse that has the same moments as the analysed filament. Prior to analysis, the dSTORM images were rotated so that pollen tubes were parallel to the x-axis.

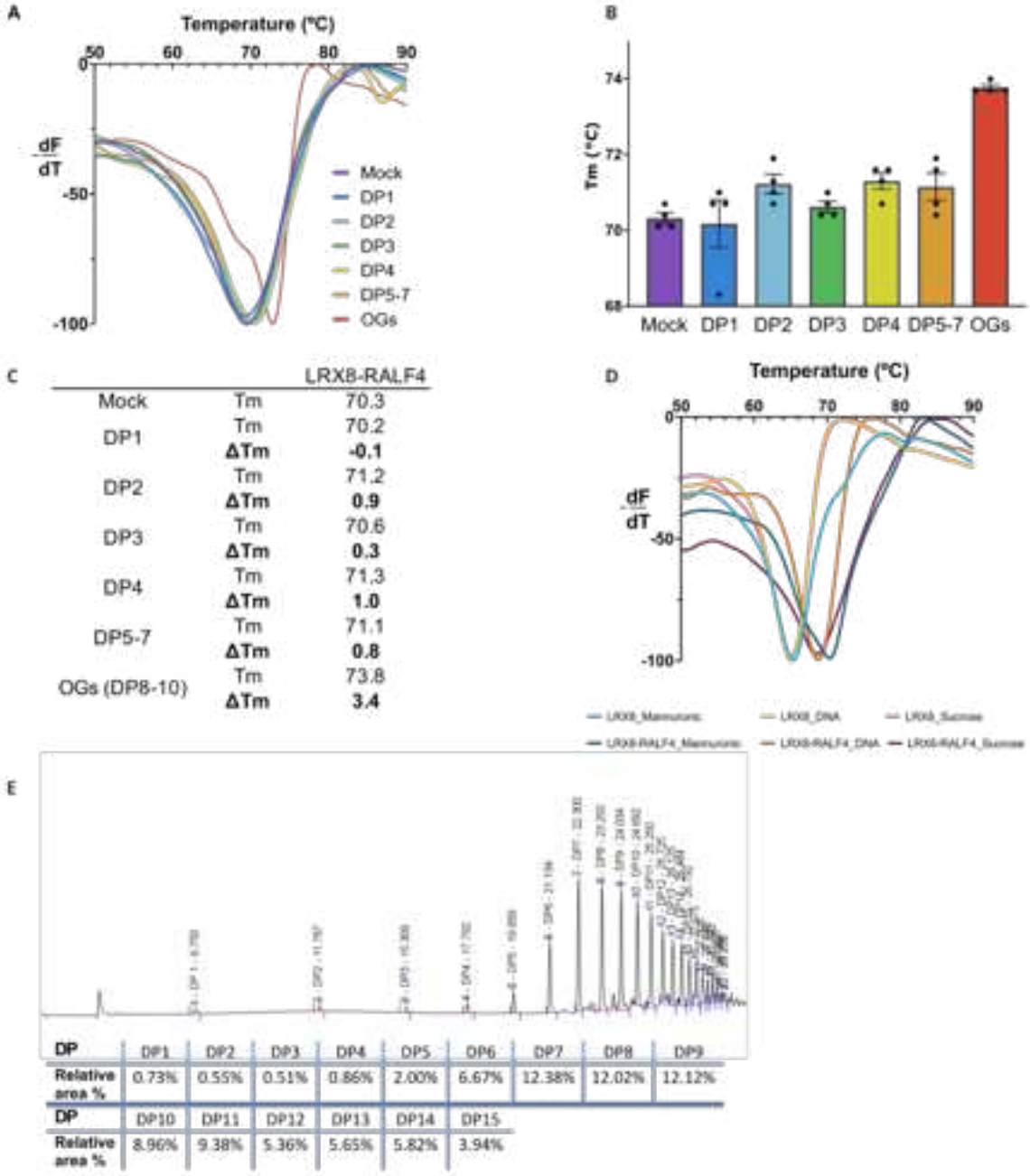

Fig. S1. LRX8-RALF4 specifically binds to longer oligomers of homogalacturonan. Thermal shift ligand-screening of homogalacturonan (HG) oligomers of different degrees of polymerization (DP) (see methods). (A, B and C) Thermal shift profiles, graph representation and summary table of the T_ms of LRX8-RALF4 *vs* HG oligomers from DP1 to DP15. (D) Thermal shift curves of LRX8-RALF4 vs different ligands represented in the summary table of Fig. 1D. (E) HPAEC-PAD analysis of the composition of the Elicityl OGs (GAT114) used in the biochemical binding experiments. Data are means ± SD of 4 independent experiments.

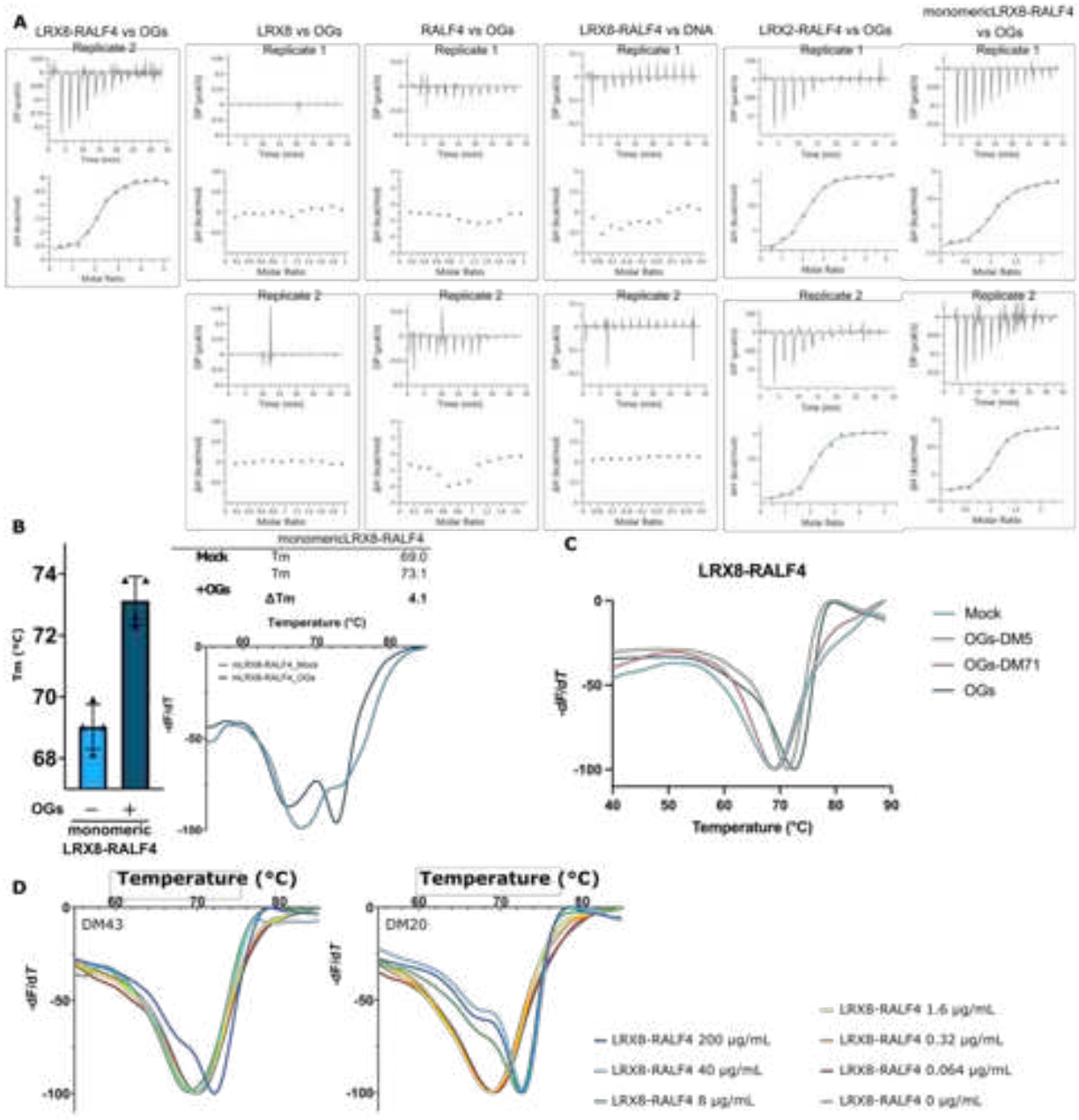

Fig. S2. LRX-bound RALF4 specifically binds homogalacturonan in a charged dependent manner. (A) ITC thermograms of the independent experiments performed and analyzed in Fig. 1E. (B) Each monomer from the LRX8-RALF4 dimeric complex binds HG. Thermal shift of mLRX8-RALF4 vs OGs. Bar representation of the melting temperature (T_m) in the presence and absence of OGs (right panel). Summary table of the ΔT_m (top). Independent profiles on the corresponding thermal shifts assays. (C-D) Thermal shift profiles corresponding to the summary tables and graphs shown in Fig. 1F,G and H. Data are means ± SD of 4 independent experiments.

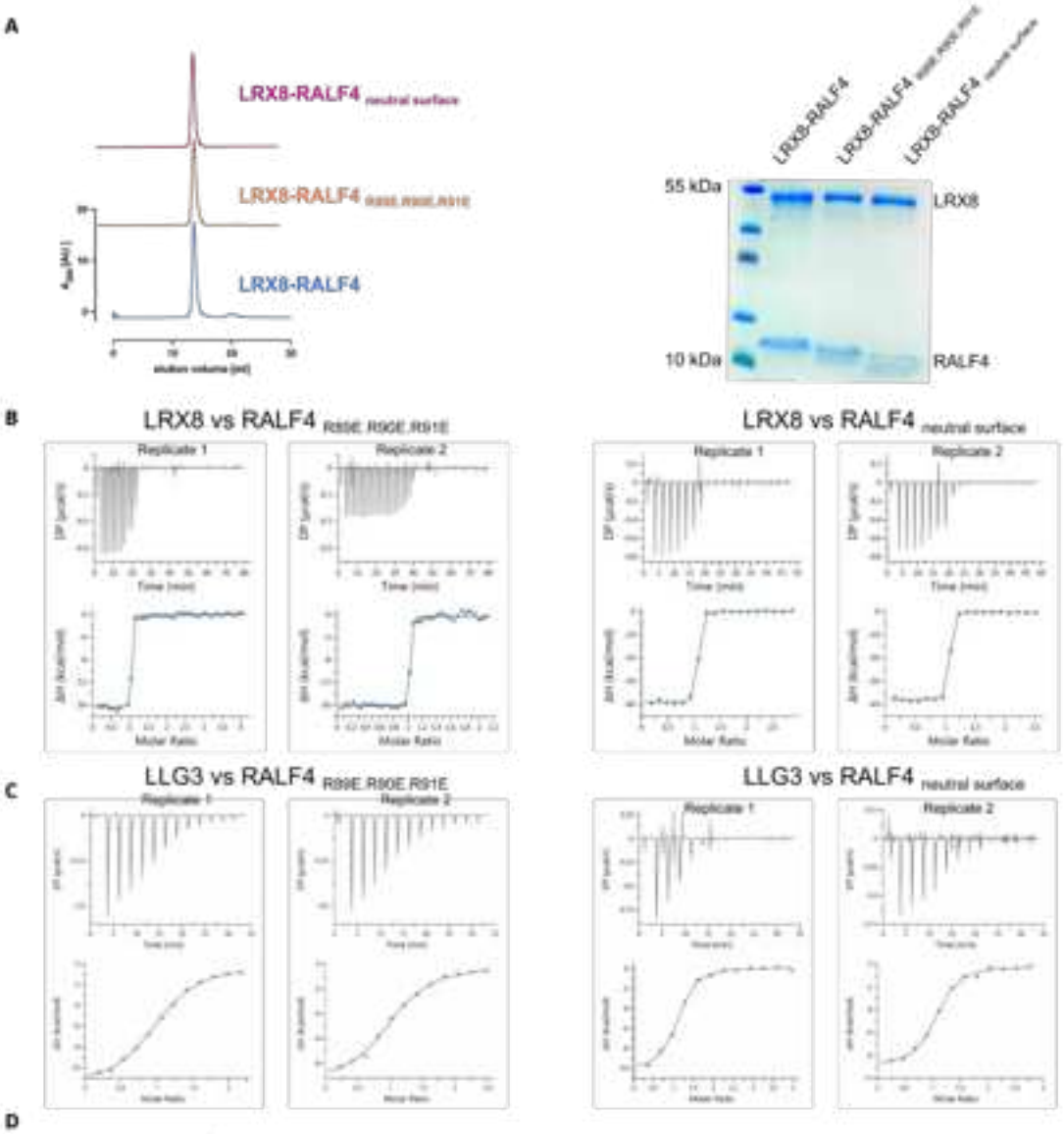

D

Ligand (syringe)	Protein (cell)	Kd (nM)	ΔH (kcal/mol)	N	pH
RALF4 R89E.R90E.R91E	LRX8	0.7 ± 0.1	-16 ± 0.5	1	5
RALF4 R89E.R90E.R91E	LLG3	2000 ± 100	-11 ± 1	1	7.5
RALF4 neutral surface	LRX8	1.5 ± 0.5	-38.5 ± 1	1	5
RALF4 neutral surface	LLG3	1000 ± 100	-10 ± 1	1	7.5

Fig. S3. RALF4 surface mutants bind LRX8 and LLG3 with wild-type affinity. (A) SEC and PAGE-SDS analysis of LRX8 in complex with RALF4 basic surface variants. (B and C) ITC thermograms of independent experiments of RALF4$_{R89E.R90E.R91E}$ and RALF4$_{neutral\ surface}$ vs pollen expressed LRX8 and LLG3, respectively. (D) ITC summary table of the experiments shown in B and C. K_d, (dissociation constant) indicates the binding affinity between the two molecules considered (in nanomolar). N indicates the reaction stoichiometry (N = 1 for a 1:1 interaction). The values indicated in the table are the mean ± SD of at least two independent experiments.

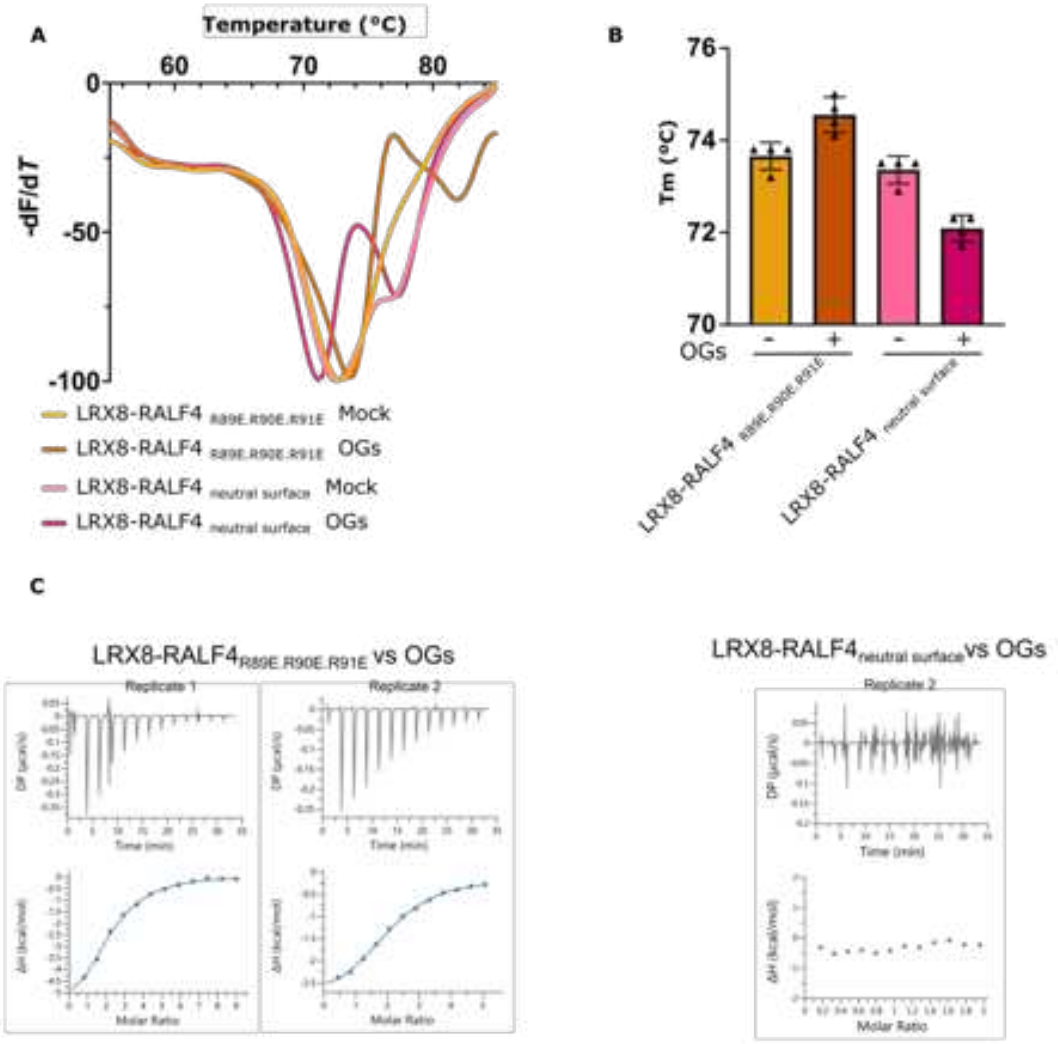

Fig. S4. ITC and thermal shift profiles of RALF4 surface mutants *vs* OGs. (A) Representative thermal shift profiles (left) and bar graph representation (B) of experiments shown in Fig. 1I. (B) Graphical representation of melting temperatures (T_m) of independent thermal shift assays shown in (A) for LRX8-RALF4 mutant complexes in the presence or absence of OGs. The data are means ± SD of 4 independent experiments. (C) ITC thermograms of the independent experiments shown in Fig. 1J.

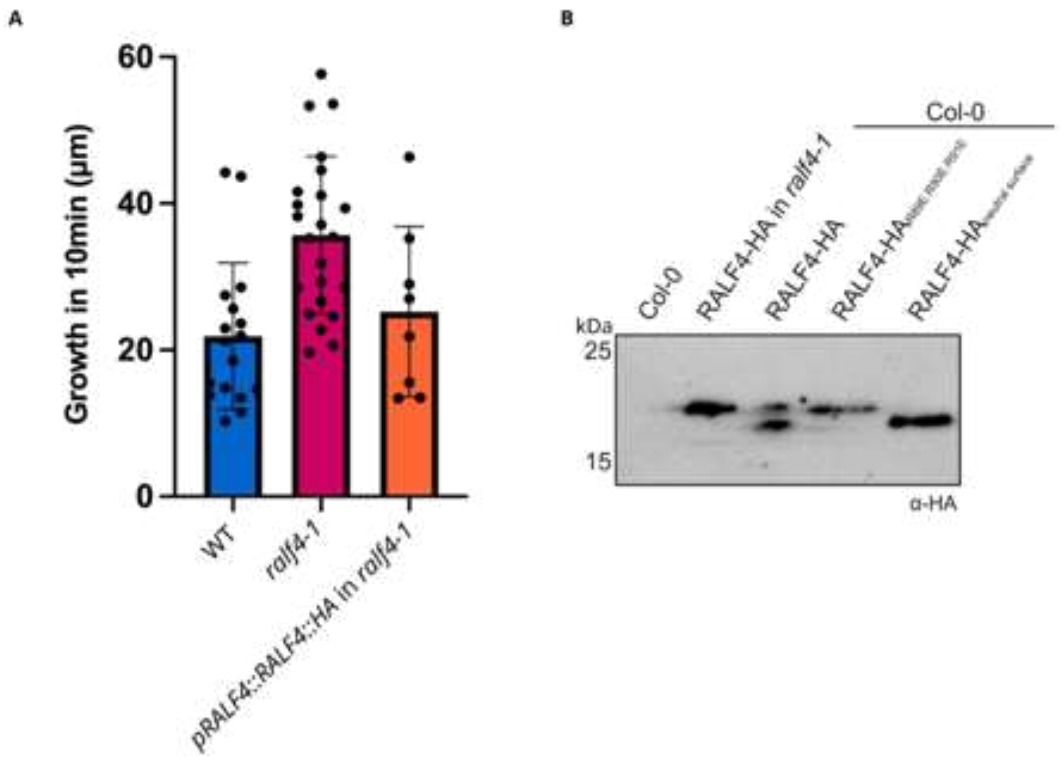

Fig. S5. *pRALF4::RALF4::HA* functionally complements the *ralf4* loss-of-function mutant. (A) Pollen tube growth speed measurements of wild type, *ralf4-1* and the *pRALF4::RALF4::HA* complementation line. *pRALF4::RALF4::HA* restores the pollen tube growth speed phenotype, described in Mecchia et al., 2017, (*9*) to wild-type levels. This indicates that the pRALF4 promoter is functional and that the HA tag at the C-terminus does not affect RALF4 function. Error bars represent SD. (B) Immunodetection of HA-tagged RALF4 and RALF4 variants in transgenic lines. Anti-HA western blot from flowers of Col-0, and transgenic lines expressing *pRALF4::RALF4::HA, pRALF4::RALF4*$_{R89E.R90E.R91E}$*::HA*, and *pRALF4::RALF4*$_{neutral\ surface}$*::HA* in *ralf4-1* and Col-0 background.

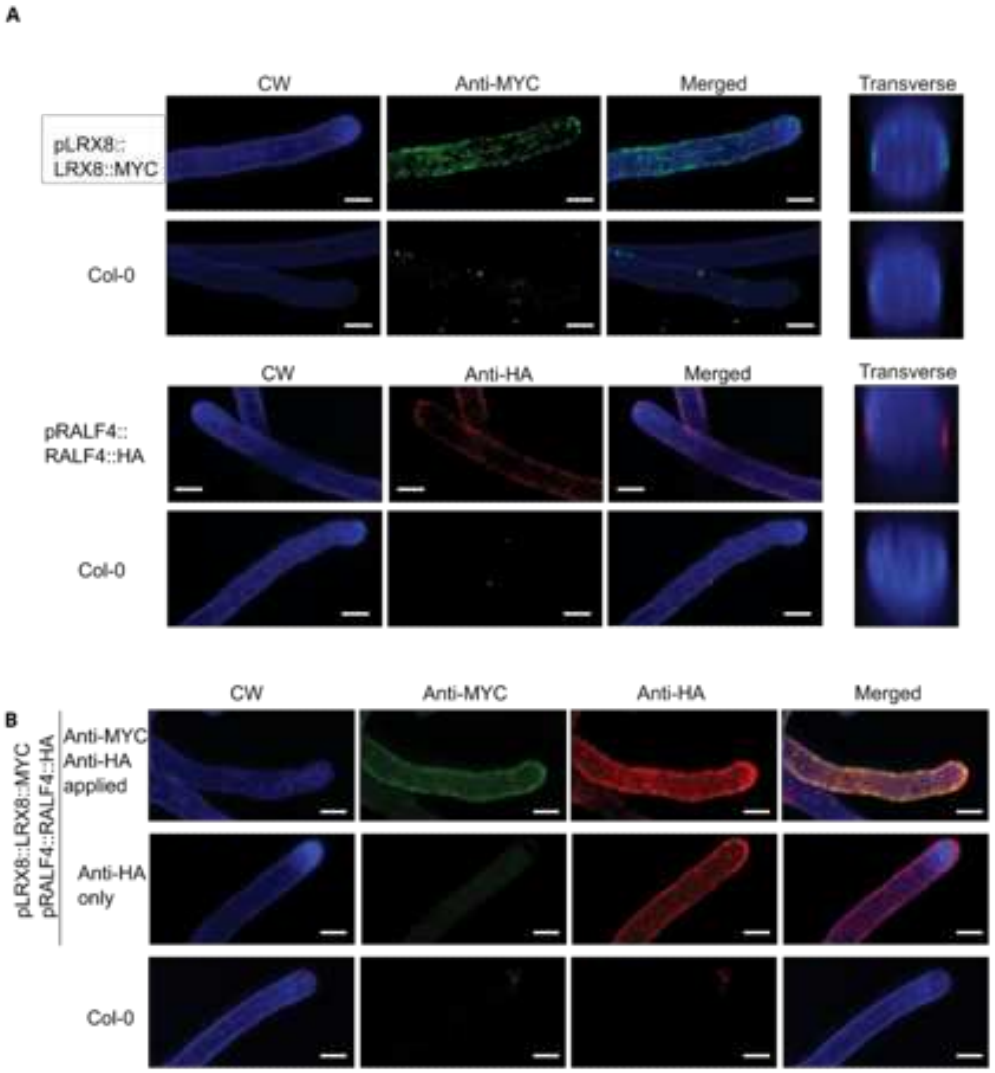

Fig. S6. LRX8 and RALF4 localize to the cell wall all along the entire pollen tube. Representative immunolabelled pollen tube images of wild-type Col-0, and transgenic lines expressing *pLRX8::LRX8::MYC* and *pRALF4::RALF4::HA* in Col-0 background. (A) Single immunolabeling of LRX8::MYC and RALF4::HA, with the corresponding test for antibody detection specificity in Col-0. Both LRX8 and RALF4 are detected in the cell wall outer layer in pollen tube transverse sections. (B) Co-immuno staining of LRX8::MYC and RALF4::HA, and antibody specificity check in different samples. Scale bar = 5 μm.

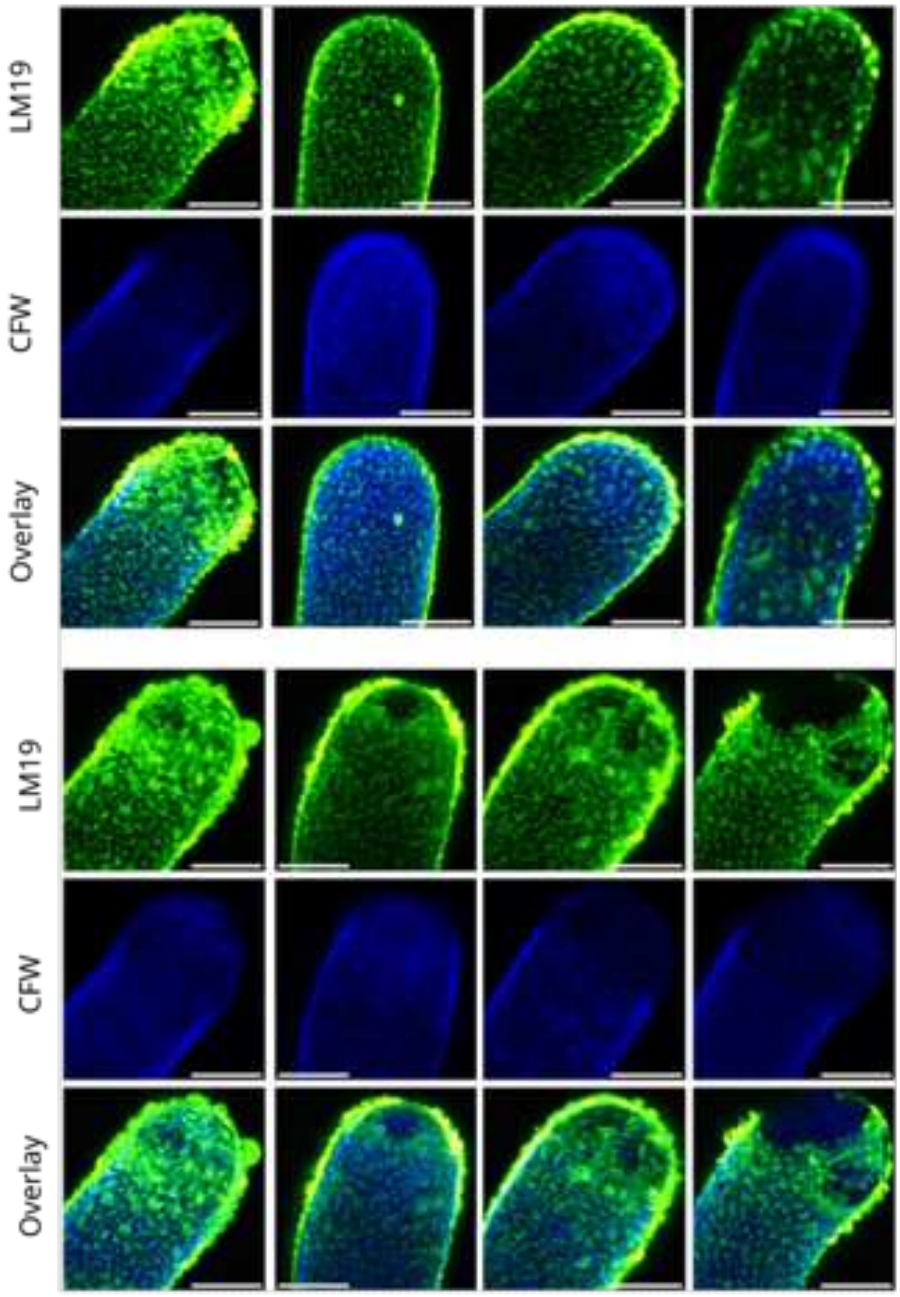

Fig. S7. Demethylesterified pectin exhibits a reticulated pattern arrangement in the shank of wild-type pollen tubes. Representative orthogonal projections of Airyscan z-stacks of the apical and transitions zone of Col-0 pollen tubes, displaying a fluorescent signal for LM19 (deesterified pectin) coupled to Alexafluor-488 (green), and Calcofluor White (blue). Scale bar 3 µm. Pollen tube shank of image 'A' is zoomed in Fig. 2F.

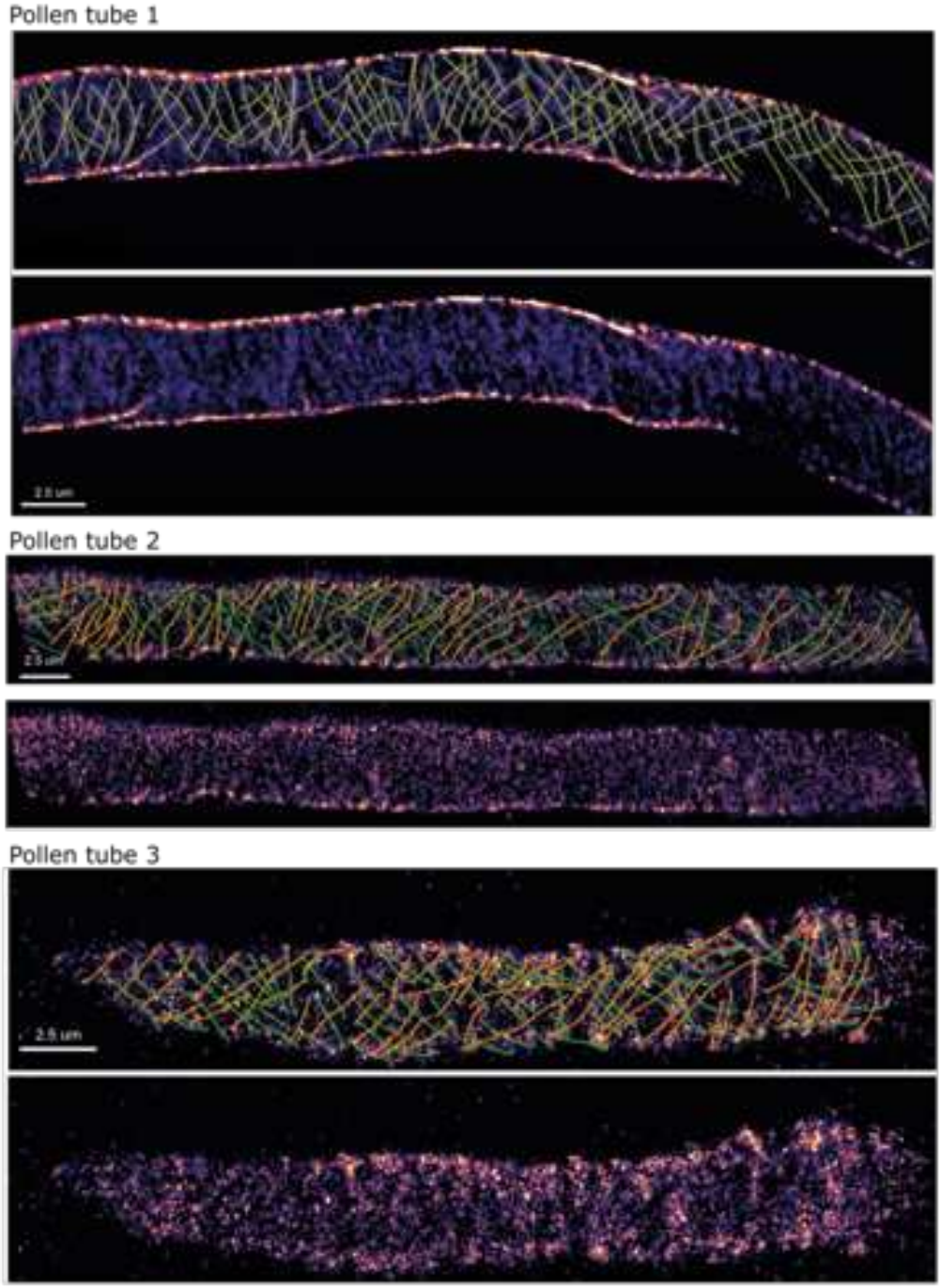

Fig. S8. Demethylesterified pectins form nanofilaments that arrange in a bimodal orientation network along wild-type pollen tubes. Representative dSTORM data acquired on independent Col-0 pollen tubes tagged with LM19 antibody and revealed with CF680 conjugated secondary antibody represented as 2D pixelated image (pixel size, 15 nm). Overlay with sketched fibers depicted in orange and green, reveals a criss-cross pattern. Scale bar 2.5 µm. A zoomed-in view of pollen tube 1 is shown in Fig. 2G.

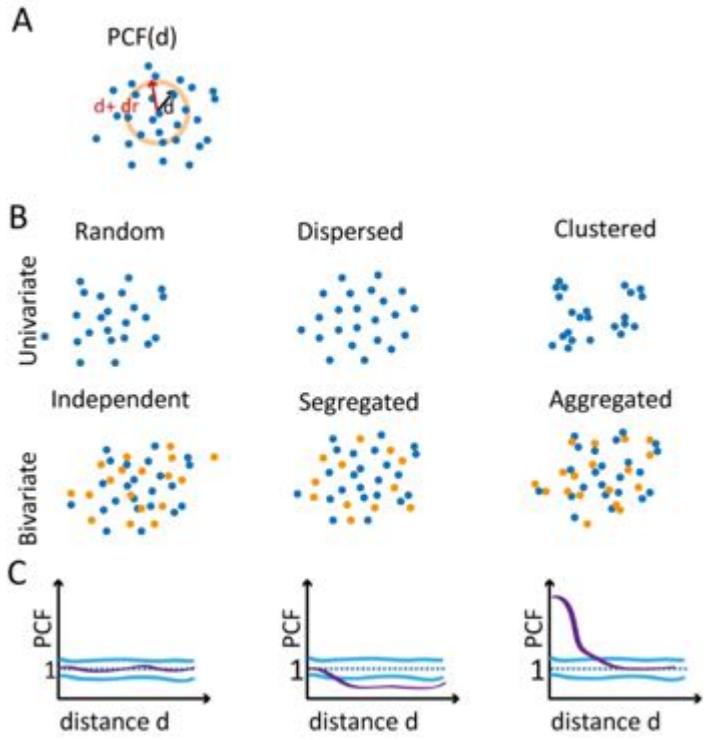

Fig. S9. Point correlation function (PCF) spatial statistical analysis. Pointilist dSTORM data consisting of 3D coordinates of points (localization of the antibody-tagged epitopes) can be considered as a spatial point pattern. This permit the analysis of dSTORM data using a spatial statistics function such as univariate (B, top row, one type of points (depicted in blue), e.g., type 1) or bivariate (B, bottom row, two type of points (depicted in blue and yellow), e.g., type 1 and 2) PCF. (A) The univariate point correlation function (PCF) can be evaluated as the number of points from pattern 1 in a thin ring centered at an arbitrary point from pattern 1 with a radius d. Equivalently, the bivariate point correlation function (PCF) can be evaluated as the number of points from pattern 2 in a thin ring centered at an arbitrary point from pattern 1 with a radius d. (B) Cartoon representation of the three scenarios that can be tested by PCF analysis. Points in the pattern 1 can be distributed randomly (independent), can be dispersed (segregated), or finally they can cluster (aggregated) with respect to points in the pattern 1 for univariate, and for points in pattern 2 for bivariate spatial point distribution. (C) The PCF (d) is evaluated for a sequence of distances (d) and usually plotted against d. If the points are distributed randomly (independently), PCF = 1, when points are dispersed (segregated) PCF < 1, when the points cluster (aggregated), PCF > 1 for univariate (bivariate) point patterning.

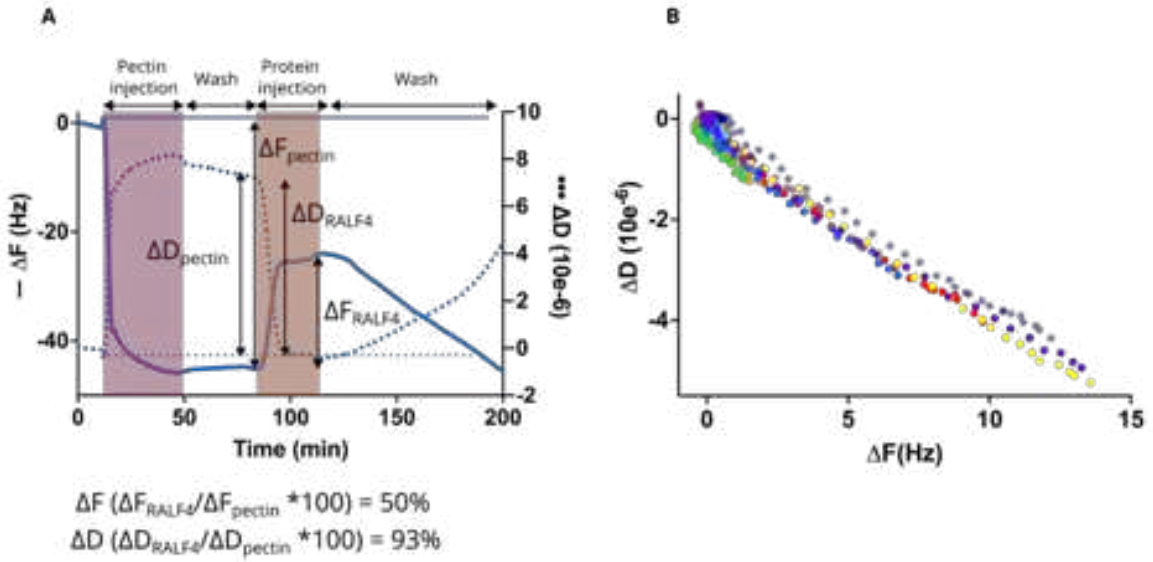

Fig. S10. Schematic representation of a QCM-D experiments and reproducibility. (A) Typical QCM-D experiment showing third harmonics of ΔF (solid blue line) and ΔD (dotted blue line) for the successive binding of a 0.1% pectin solution poured over (Degree of Methylation (DM43) a gold-topped quartz coated with a polyallylamine hydrochloride (PAH) layer. This procedure was followed by a washing step to remove the excess of uncoupled pectin. The indicated protein in each experiment was injected over the pectin layer, followed by a washing step. In the case of the experiment shown, a solution of RALF4 at 1µg/ml. Pink and orange zones depict the period during which pectin and protein solutions, RALF4 in this case, were injected, respectively. Upon pectin application, ΔF decreases and ΔD increases, reflecting an increase in mass and a decrease in stiffness, respectively, related to the formation of a pectin layer. Upon RALF4 application, this behavior reverses (ΔF increases and ΔD decreases), indicating the RALF4-induced dewatering and a subsequent stiffening of the pectin layer. The process slowly reverts upon washing, indicating the reversibility of the RALF4-induced pectin condensation when not bound to LRX8. (B) Independent experiments using different batches of pectin and protein show consistent results. ΔD *vs* ΔF of 10 independent binding experiments of RALF4 to DM43 pectin layers. The zero value refers to the ΔF and ΔD values of the pectin layers before the addition of RALF4. Although the individual experiments may show variations in ΔF and ΔD profiles depending on the quartz, the pectin or the protein preparation; the ΔD/ΔF ratio of independent experiments show a remarkable robustness across experiments. Colors refer to independent experiments.

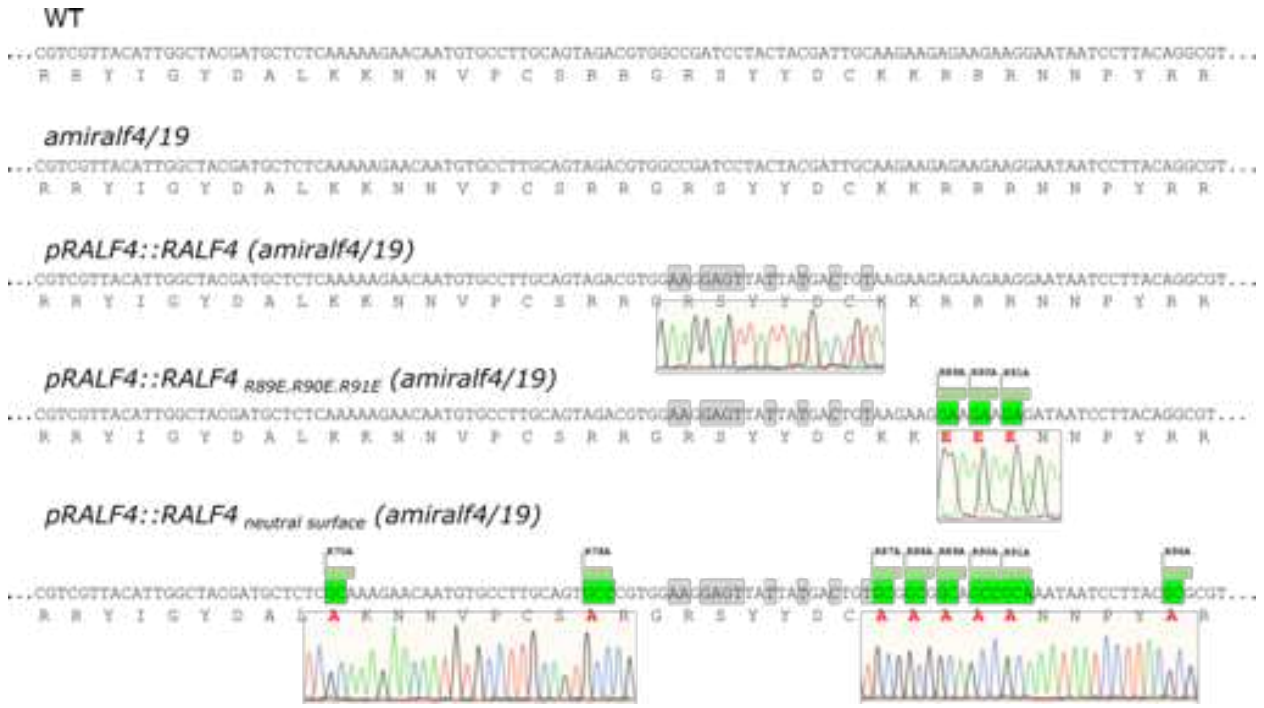

Fig. S11. Sequencing and characterization of complementation lines with different RALF4 variants. Sequencing data of cDNA amplification of wild type Col-0 and *amiralf4/19* complemented with an amiR-resistant version of $RALF4_{WT}$, $RALF4_{R89E.R90E.R91E}$ and $RALF4_{neutral\ surface}$ under the control of the native *pRALF4* promoter.

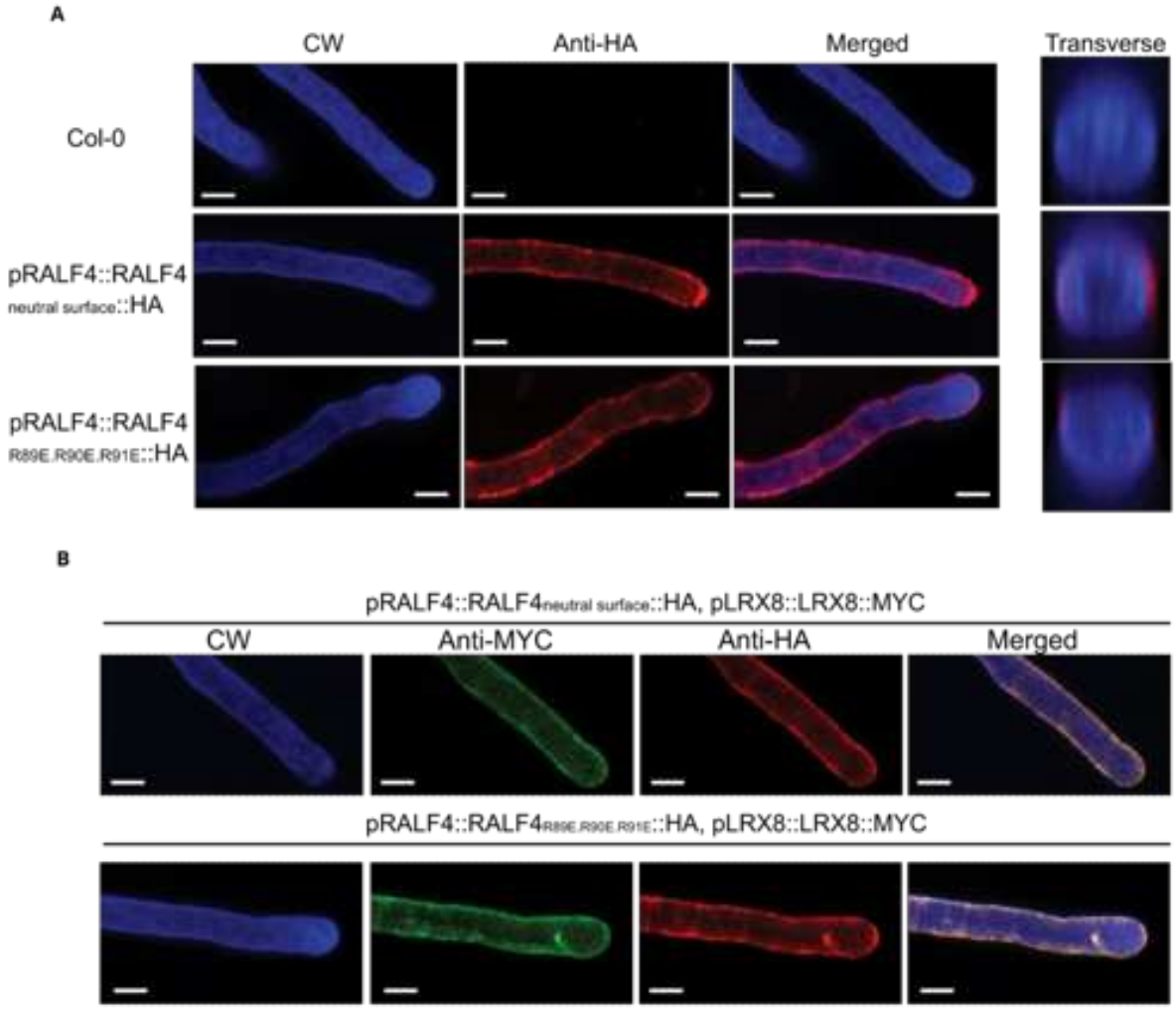

Fig S12. RALF4 surface mutants localize to the pollen tube cell wall and colocalize with LRX8. (A) RALF4$_{R89E.R90E.R91E}$::HA and RALF4$_{neutral\ surface}$::HA localize to the cell wall along the pollen tube. Representative immunolabeled pollen tube images of Col-0, and transgenic lines expressing *pRALF4::RALF4*$_{R89E.R90E.R91E}$*::HA* , and *pRALF4::RALF4*$_{neutral\ surface}$*::HA* in Col-0 background. (B) RALF4 polycationic surface variants co-localize with LRX8 in the pollen tube cell wall. Representative immunolabeled pollen tube images of transgenic lines expressing LRX8-MYC and RALF4 $_{R89E.R90E.R91E}$::HA or RALF4 $_{neutral\ surface}$::HA under the *pRALF4* promoter. Scale bar = 5 µm.

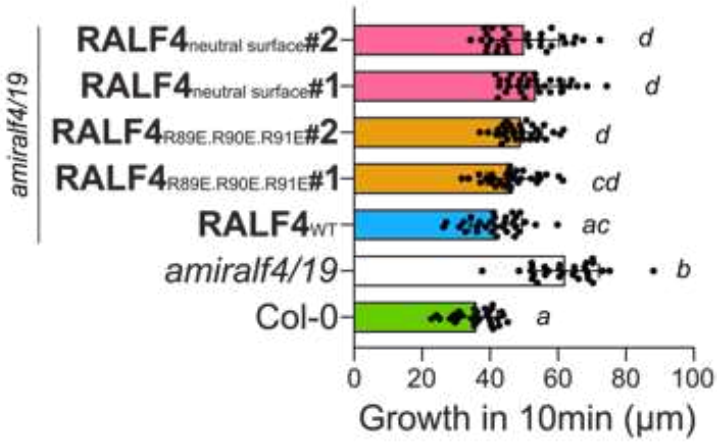

Fig S13. RALF4 basic-surface mutants show an increased growth speed compared to wild-type pollen tubes. RALF4 surface mutants fail to fully complement the fast *amiralf4/19* pollen tube growth phenotype. In vitro pollen tube growth was measured in 10 min for Col-0 (WT), *amiralf4/19, amiralf4/19 pRALF4::RALF4*$_{WT}$, *amiralf4/19 pRALF4::RALF4*$_{R89E.R90E.R91E}$ and *amiralf4/19 pRALF4::RALF4*$_{neutral\ surface}$ lines. Error bars are SD, 30 pollen tubes per n, n=3. Statistical tests were performed using one-way ANOVA ($p<0.0001$) followed by a multiple comparison using Tukey HSD test.

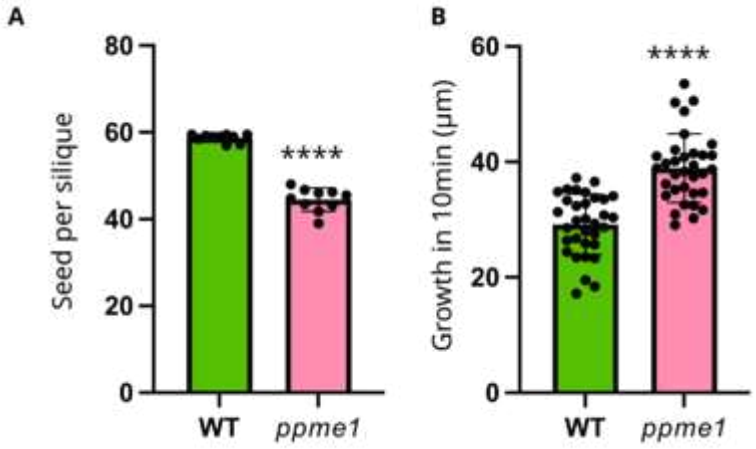

Fig. S14. Characterization of the *ppme1* loss-of-function pollen tube mutant. (A) and (B) The *ppme1* mutant exhibits altered fertility and pollen tube growth speed phenotypes. Seeds per silique count for Col-0 and *ppme1* mutants were measured. A total of 10 siliques per plant were counted, n=4. (B) Growth distances were measured for both Col-0 and *ppme1* mutant pollen tubes *in vitro*. Error bars are SD, 30 pollen tubes were measured per n, n=3. Statistical tests were performed using two-way ANOVA ($p<0.0001$).

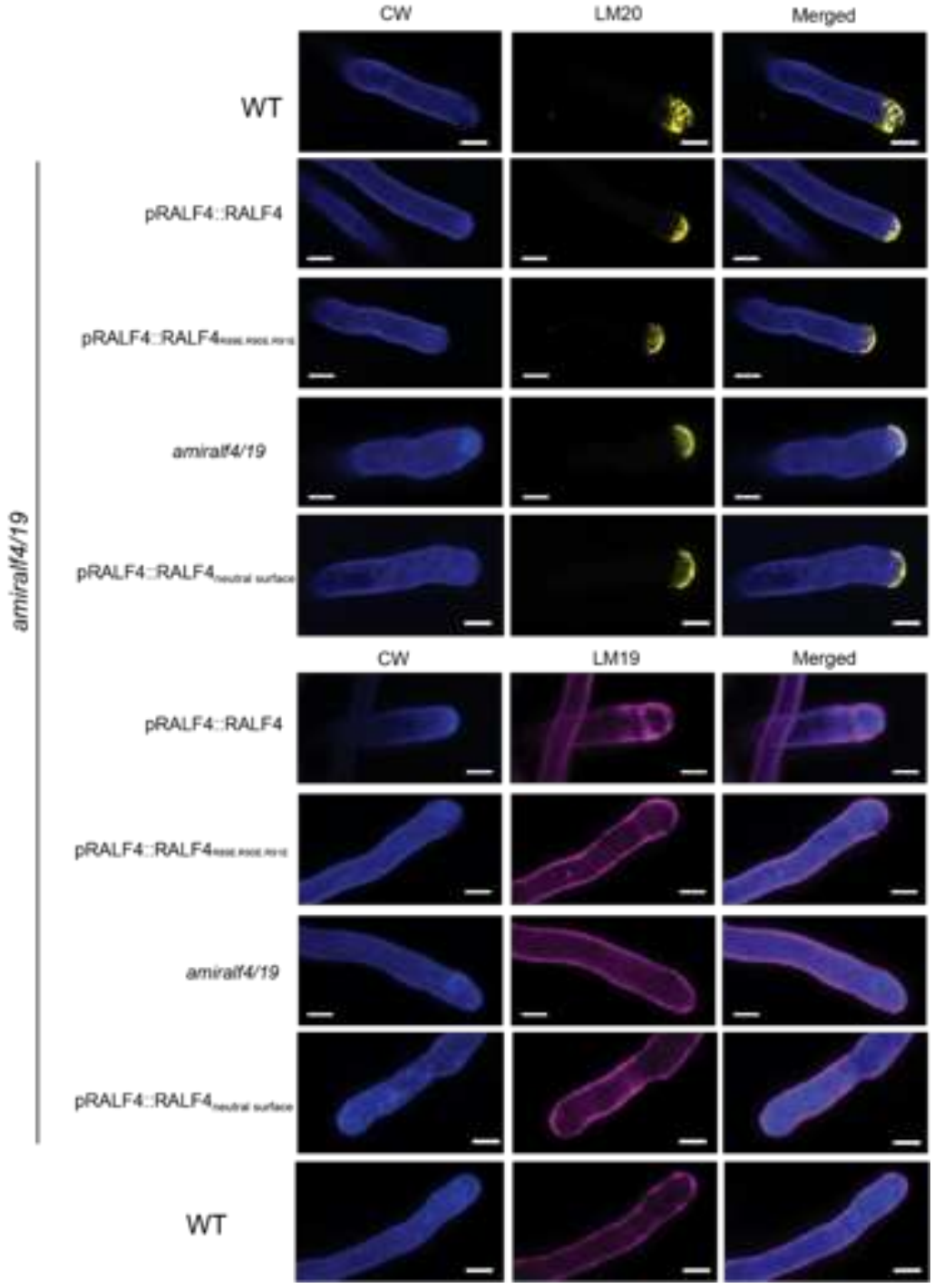

Fig. S15. Pectin distribution of esterified and de-methylesterified pectins is unchanged in pollen tubes of the RALF4 surface mutants. Representative immunolabeled images of *amiralf4/19*, and complementing lines expressing *pRALF4::RALF4*$_{WT}$, *pRALF4::RALF4*$_{R89E.R90E.R91E}$ and *pRALF4::RALF4*$_{neutral\ surface}$; labelled either with LM20, fully-methylesterified pectin or LM19, de-methylesterified pectin. Scale bar = 5 μm.

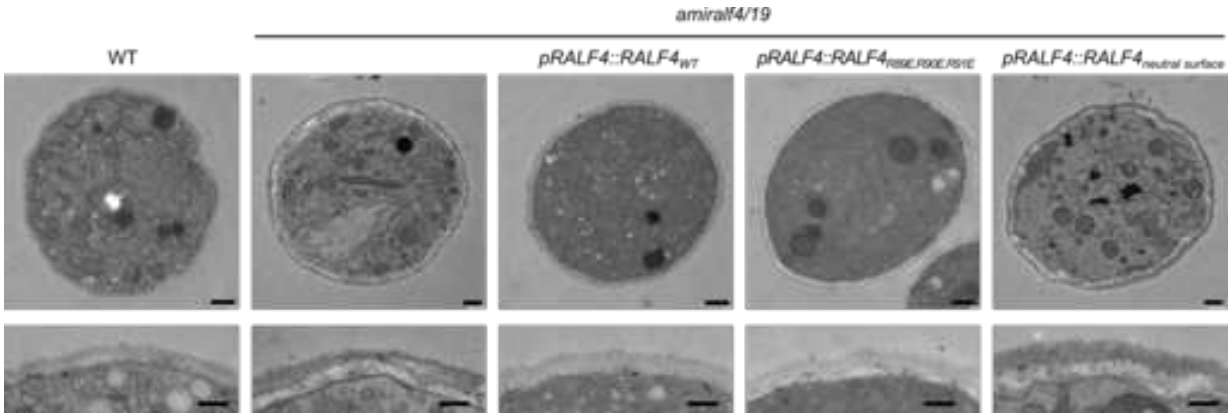

Fig. S16. **RALF4 polycationic surface mutants exhibit a defective cell wall architecture.** Representative cross-section TEM images of pollen tubes from complementation lines expressing *pRALF4::RALF4*, *pRALF4::RALF4*$_{R89E.R90E.R91E}$, and *pRALF4::RALF4*$_{neutral\ surface}$ transgenes, shown in Fig. 4A. Immunogold labeled dots indicate callose, the darker layer represents the primary cell wall. Scale bar = 500 nm (top) and 200 nm (bottom). Sections were taken transversely around ~10 μm from the tip.

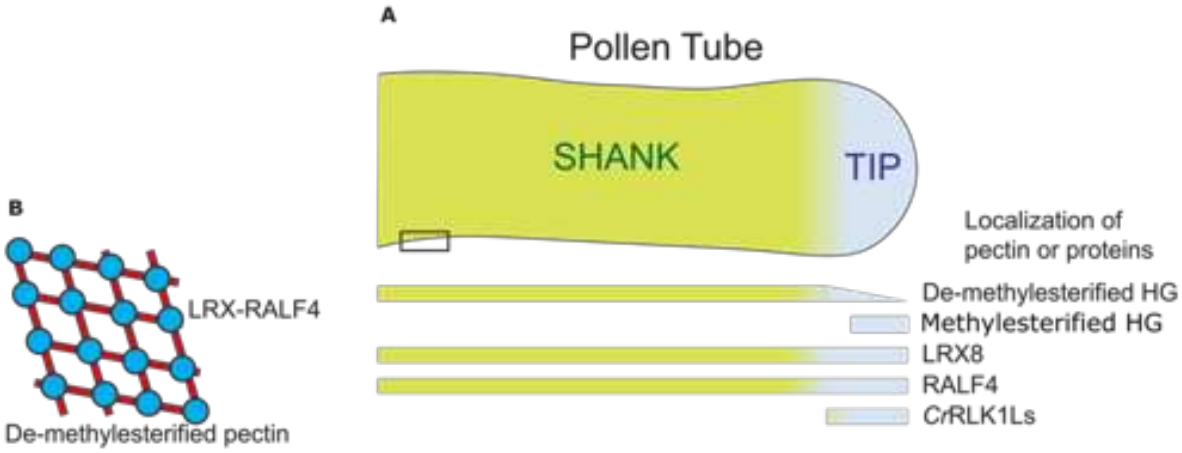

Fig. S17. Conceptual mechanism for pectin network assembly via the pollen tube LRX-RALF4 hetero-tetrameric complex. (A) Localization pattern of esterified and demethylesterified HG, together with cell wall integrity signaling components in pollen tubes. The tip and shank are colored in blue or light green, respectively. The bar diagram depicts the spatial profile of cell wall integrity proteins and pectins with different degree of methylation. (B) Cartoon representation of the reticulated network formed by the LRX8-RALF4-pectin interaction. Demethylesterified pectin is depicted as red lines and the LRX8-RALF4 complex in blue circles.

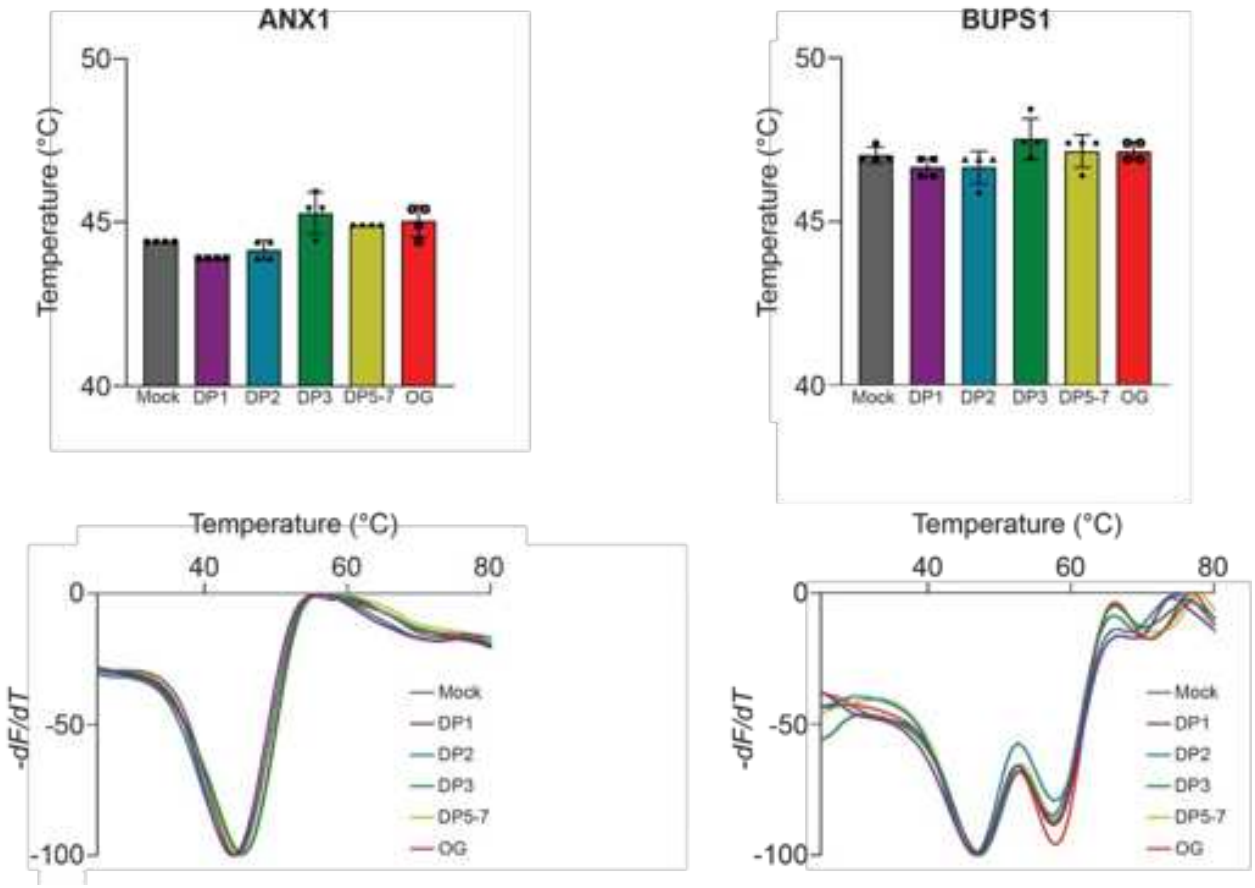

Fig. S18 ANX1 and BUPS1 do not associate with OGs with high affinity, forming a stable complex. Thermal shift ligand-screening of HG oligomers of different degrees of polymerization (DP) (see methods). OGs from 1 to ~15 mers do not induce a T_m increase with ANX1 or BUPS1. Thermal shift profiles (bottom) and graph representation (top) of ANX1 and BUPS1 T_ms in the absence and presence of homogalacturonan oligomers from DP1-DP15. Data are means ± SD, n=4